AN ABSTRACT OF THE THESIS OF

Joshua L. Strom for the degree of Master of Science in Mechanical Engineering
presented on June 4, 2012

Title: An Investigation of Transition from Penetration to Deflection in the Fracture of Bi-Material Interfaces

Abstract approved:

_____

John P. Parmigiani

The problem of determining whether a crack impinging on an interface will penetrate into the substrate or deflect along the interface is vital to the effective design of layered and composite material systems. Of particular interest is the transition between crack propagation by penetration through an interface and deflection along an interface. There has been a great deal of work done on this problem to determine what parameters and formulations are necessary to accurately determine under what conditions penetration-deflection transition will occur. Previous work has studied this problem using stress-based, energy-based, and combined stress-energy-based approaches. Most recently, a combined stress-energy-based approach was implemented via a cohesive-zone formulation; this work showed the conceptual basis and correctness of the cohesive-zone approach, however only presented limited investigation into the behavior penetration-deflection transition.

Work presented here expands this investigation on transition, exposing trends and behavior that emerge as certain dimensionless groups are varied. Principles of linear elastic fracture mechanics and, as in previous work, cohesive-theory are applied to a bi-material system in tension through the use of the commercial finite element analysis package ABAQUS. Dimensionless groups, including strength ratios, toughness ratios, fracture-length scales, and substrate toughness scales are varied systematically to show resulting system behavior in a generalized fashion. In using the cohesive-zone method, aspects of previous stress-based and energy-based formulations are reproduced. It is also shown where these formulations cease to be valid, revealing unique and previously undetected transitional interface fracture behavior. The results presented here will prove valuable in interface design as the described generalized trends can be used as references in the design of new layered and composite systems.

An Investigation of Transition from Penetration to Deflection in the Fracture of Bi-Material Interfaces

by
Joshua L. Strom

A THESIS

submitted to

Oregon State University

in partial fulfillment of
the requirements of the
degree of

Master of Science

Presented June 4, 2012
Commencement June 2013

Master of Science thesis of Joshua L. Strom presented on June 4, 2012

APPROVED:

Major Professor, representing Mechanical Engineering

Head of the School of Mechanical, Industrial, and Manufacturing Engineering

---

Dean of the Graduate School

I understand that my thesis will become part of the permanent collection of Oregon State University libraries. My signature below authorizes release of my thesis to any reader upon request.

Joshua L. Strom, Author

ACKNOWLEDGEMENTS

I would like to express my sincere appreciation to my advisor, Dr. John Parmigiani, for his help throughout my enrollment at Oregon State University. As a graduate student, my academic growth was rooted in his guidance and facilitated by his insight. Further, without his support, my graduate pursuance simply would not have been possible.

My fellow students in Dr. Parmigiani's Computational Mechanics and Applied Design group deserve my most sincere thanks for their encouragement and their sharing of a vast collective knowledge.

I would also like to thank Dr. Timothy Kennedy, Dr. Jamie Kruzic, and Dr. Bill Warnes for their unparalleled instruction and advice in and out of the classroom.

Finally I would like to thank my friends and family for their love, support, and encouragement; without them, success would be near impossible and if achieved, would be without merit.

TABLE OF CONTENTS

TABLE OF CONTENTS (Continued)

Page

LIST OF FIGURES

Figure Page

LIST OF FIGURES (Continued)

Figure Page

LIST OF FIGURES (Continued)

Figure Page

An Investigation of Transition from Penetration to Deflection in the Fracture of Bi-Material Interfaces

1. Introduction

Sound engineering of layered and composite material systems requires a firm understanding of material behavior at interfaces. The integrity of many layered materials, such as composite, laminate, and thin film systems, depends on crack behavior at intra-system interfaces. When these systems are loaded, it is at the interfaces where failure is common. It follows that, to be able to design these composite materials to their maximum potential, it is important to understand the failure mechanisms at these interfaces. An important failure mechanism to consider is fracture.

Fracture is a common failure mechanism in composite material systems and, through design, can be counteracted by implementing toughening mechanisms. As the system is loaded and begins to fail, micro-cracking forms and grows with applied load. With increasing applied load, cracks extend until they ultimately reach an interface. In composite materials, the interface lies between the matrix and fiber; in layered materials, the interface is simply between layers. During fracture, it is at these interfaces that toughening mechanisms are apparent. Mechanisms, such as fiber-bridging (Ruhle et al. [1]) and inter-material friction (Cambell et al. [2]), are known to increase fracture resistance. These mechanisms can be achieved in engineered materials through understanding crack behavior near interfaces. These mechanisms rely on crack propagation by deflection along the interface. Deflection itself has also

been shown to be an effective means of toughening by Faber and Evans [3]. It is therefore of particular importance to understand whether a crack impinging upon an interface will propagate by deflection along the interface or penetration through the interface.

2. Penetration versus Deflection

The overall fracture properties of composite materials depend upon whether penetration or deflection occurs. That is, whether a crack impinging an interface will tend to penetrate through the interface and into the substrate material or deflect and propagate along the interface. Figure 1 illustrates penetration versus deflection as applied to a bi-material system in which two materials (a film and a substrate) are bonded. Figure 1(a) illustrates a crack in the film normally impinging an interface. Depending on the material properties of the film, interface, and substrate, the crack may penetrate into the substrate (Figure 1(b)) or deflect at a right-angle along the interface (Figure 1(c)). For a film and substrate both isotropic and homogeneous under the loading shown, the impinging crack can only propagate at a parallel (penetrating) or normal (deflecting) path. Determining whether penetration or deflection will occur has been studied using several methods.

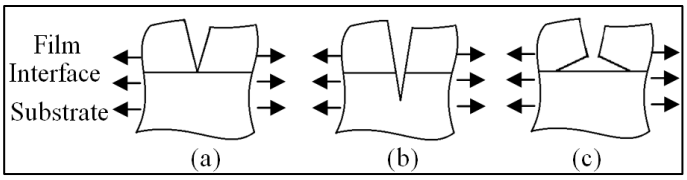

Figure 1: Semi-infinite interfacial crack geometries. (a) Crack normally impinging interface. (b) Crack penetrating through interface into substrate. (c) Crack deflecting along interface.

3. Literature Review

Interface fracture has been examined using three main approaches: stress-based, energy-based, and combined stress-energy-based. The result of a stress-based approach is a critical strength ratio (strength of substrate material to strength of interface material) which determines penetration or deflection. Similarly, the energy based approaches result in a critical toughness ratio (critical fracture energy of substrate material to critical fracture energy of interface material) which determines penetration or deflection. In a combined stress-energy approach, the resulting penetration versus deflection criteria is a relationship of strength and toughness which separates penetration from deflection.

3.1 Stress-Based Work

Stress-based formulations develop stress criteria in the penetrating and deflecting directions which can then be compared to critical material strengths in order to determine which failure has occurred. Early work by Cook and Gordon [4] used a formulation in which the stress field immediately ahead of a crack was examined. By extracting stresses normal to each other immediately ahead of the crack (the stress

immediately ahead of the crack being the stress in the penetrating direction), a critical ratio of substrate to interface strength of $\sigma_s/\sigma_i \approx 5$ was derived. This ratio describes a critical set of material strengths in which a penetrating case would switch to a deflecting case. The work by Gupta et. al. [5] is a great expansion of the work by Cook and Gordon [4], taking the stress field technique and applying it to a system having an interface between two anisotropic materials. For two isotropic materials, however, having same elastic properties, elastic modulus and Poisson's ratio ($E_1 = E_2$, $\nu_1 = \nu_2$), a critical strength ratio of $\sigma_s/\sigma_i \approx 3$ was extracted. These approaches take only the strengths of the interface and bulk materials into account; they do not consider any energy (work of fracture, or toughness) aspects of the material.

3.2 Energy-Based Work

Based on the methods described by linear elastic fracture mechanics (LEFM), several energy-based solutions exist for determining whether a crack impinging on an interface will penetrate or deflect. The work of He and Hutchinson [6] is a popular energy-based approach for determining penetration versus deflection. This method examines energy release rates associated with kinks extending from a main crack in the penetrating, G_p, and deflecting, G_d, directions. This is performed through examining penetrating and deflecting geometries independently. Figure 2 shows the two geometries considered by He and Hutchinson [6]; Figure 2(a) shows the penetrating geometry and Figure 2(b) shows the deflecting geometry. Results are then

compared to each other to arrive at a theoretical ratio of energy release rates, G_p/G_d.

This ratio is then taken to equate to the critical substrate to interface toughness ratio which separates penetration from deflection. He and Hutchinson [6] formulate this transition toughness ratio to be $\Gamma_s/\Gamma_i \approx 4$. Because two separate geometries are used to analyze this penetration versus deflection, this approach will be referred to as a two-geometry approach.

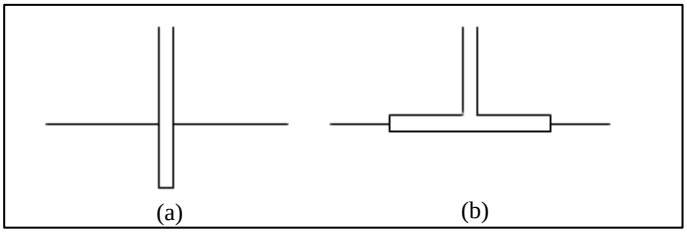

Figure 2: Distinctly separate geometries used in energy based formulations. (a) Penetrating kink. (b) Deflecting kink.

Per the derivation presented in Appendix B, Equations (16) and (17) are plotted in Figure 3 as a function of toughness ratio, Γ_s/Γ_i. This adaptation of the results of He and Hutchinson [6] represents the load carrying capacity for the associated geometry. On this plot, the curve with lower associated fracture load represents the mode of failure. Further, the point at which the curves intersect represents the critical toughness ratio for penetration/deflection transition. Figure 3 recaptures the critical toughness ratio of $\Gamma_s/\Gamma_i \cong 4$, as described in the work of He and Hutchinson [6]. This

point corresponds to the conditions under which the same applied load will cause either a kink in the substrate, Figure 2(a), to propagate or a kink along the interface, Figure 2(b) to propagate.

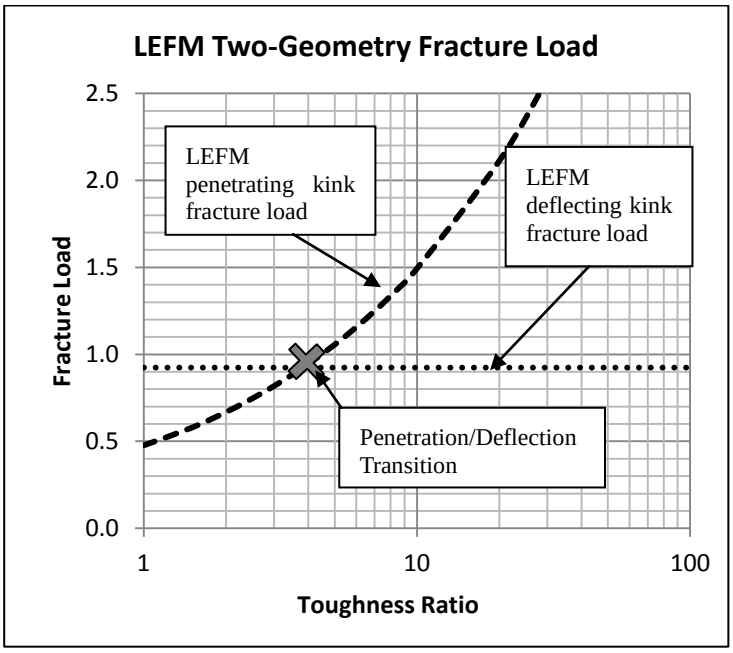

Figure 3: Results of LEFM formulation by He and Hutchinson [6]. The intersection of the two curves marks the transition toughness ratio.

Three other energy formulations are those of Leguillon et al. [7], Tullock et. al. [8], and Matinez and Gupta [9]. These formulations use the same approach as that of He and Hutchinson [6]; they independently develop energy release rates for the penetrating and deflecting geometries and compare them to each other. That is, a two-geometry approach is used.

3.3 Combined Stress-Energy-Based Work

Most recently, stress and energy have been examined in combination to determine penetration versus deflection. The combined stress-energy-based approach was first used to explore the penetration versus deflection problem for a normally-incident crack in work by Parmigiani and Thouless [10]. In this work, cohesive-zone modeling was used to define regions at the crack tip in the penetrating and deflecting directions that utilize both stress and energy components in order to determine fracture behavior. Following the aforementioned work by Parmigiani and Thouless [10], a subsequent combined stress-energy approach can be found in work by Martin et al. [11]. In this work, an analytical formulation of fracture for the case of a main crack approaching, but never reaching, an interface was developed. This combined approach is advantageous as it considers both material strength and toughness, encompassing all solutions yielded by either single approach. Unfortunately, however, the combined approach is relatively unfamiliar as it has only recently been explored. This may be due to the difficulties associated with implementing such a formulation, often requiring the use of computational methods.

3.4 Present Work

Three approaches have been described above to analyze penetration versus deflection; these approaches are stress-based, energy-based, and stress-energy-based. Though these approaches analyze the same problem, they use different formulations and yield different criteria which distinguish penetration from deflection. That is, the

stress-based formulation yields a critical strength ratio, the energy-based formulation yields a critical toughness ratio, and the stress-energy-based formulation yields a mixed strength and toughness criterion. The significance of this difference is that between the stress-based and energy-based approaches, the penetration versus deflection criteria is defined by totally different material properties. And thus, by using one approach over the other, the alternate material property is left completely disregarded; this may yield inaccurate analyses. In work by Leguillon [12], it is shown that stress or energy based approaches alone are not sufficient in determining crack behavior at an interface; both stress and energy must be considered together in order to understand interfacial crack propagation. This is achieved by showing specifically that the interfacial-fracture solution space is bounded on one end by stress-based formulations and on the other by energy-based formulations; this work is also collaborated by experimental results. The stress-and-energy-based approach provides a complete solution and thus a link between these bounds.

The focus of the work presented here will be to compare these three approaches under conditions for which crack-propagation changes from penetration to deflection (or vice versa). That is, what material property values (strength, toughness, or both) are required for crack propagation to change from penetration through an interface to deflection along an interface (or vice versa). This change will be referred to as "transition". Predictions of transition conditions are a common use of penetration versus deflection criteria and provide a useful context for demonstrating the necessity of a strength-energy criteria.

4. Method

Here, the methods used in work presented here are described. A cohesive-zone approach (CZ, combined strength-energy approach) is used and deployed using finite element analysis.

4.1 Nomenclature

Below is a list and explanation of parameters used throughout the body of this work.

h: Film height
d: Substrate height
l: Model half-length
k_i: Interface kink length
k_s: Substrate kink length
$\sigma_{applied}$: Remote applied stress
$\bar{E}_f$: Film elastic modulus
ν_f: Film Poisson's ratio
$\bar{E}_s$: Substrate elastic modulus
ν_s: Substrate Poisson's ratio
Γ_s: Substrate toughness
$\hat{\sigma}_s$: Substrate normal cohesive strength
K_p: Penetrating stress intensity factor
K_d: Deflecting stress intensity factor
G_p: Energy release rate in the penetrating direction
G_d: Energy release rate in the deflecting direction
Γ_{iI}: Interface mode-I toughness
Γ_{iII}: Interface mode-II toughness
$\hat{\sigma}_i$: Interface normal cohesive strength
$\hat{\tau}_i$: Interface shear cohesive strength

4.2 Cohesive-Zone Modeling

The CZ method used here is the same as that used in the work by Parmigiani and Thouless [10]. This work provided the basis for and showed the correctness of the CZ approach as applied to interface fracture.

Cohesive theory was first developed in work by Dugdale [13] and Barenblatt [14] in the early 1960's. In cohesive theory, a region of assumed crack extension, called the cohesive-zone (CZ), is governed by a stress versus crack tip opening displacement (CTOD) relationship. This relationship is called a traction separation law (TSL). It is important to note that by expressing stress in terms of displacement, the resulting area under the TSL curve is the energy released by fracture (material toughness). It is this constitutive relationship that defines the behavior of the crack extension in cohesive modeling.

The TSL used in present work is trapezoidal in shape. This law was chosen as it is the same used successfully in work by Parmigaini and Thouless [10]. Further, since normal and shear stresses exist in this present problem (shear stresses are present in the interface), a TSL capable of modeling mixed-mode loading must be used. Moreover, the TSL used here has independent components for Mode-I and Mode-II loading. The ability to define Mode-I and Mode-II properties (strength and toughness) independently has been shown to accurately capture experimental results (Yang and Thouless [15], Kafkalidis and Thouless [16], and Li et al. [17]). Figure 4 shows the trapezoidal geometry of the TSL's used in this work. From left to right, the law first

defines a region of linear elasticity; this is maintained until displacement reaches δ_1. A region of perfect plasticity is followed (the horizontal region of the TSL) and is maintained until δ_2 is reached. The final portion of the law defines a region of linear stiffness degradation which defines the load-carrying ability to diminish to zero at the critical displacement δ_c.

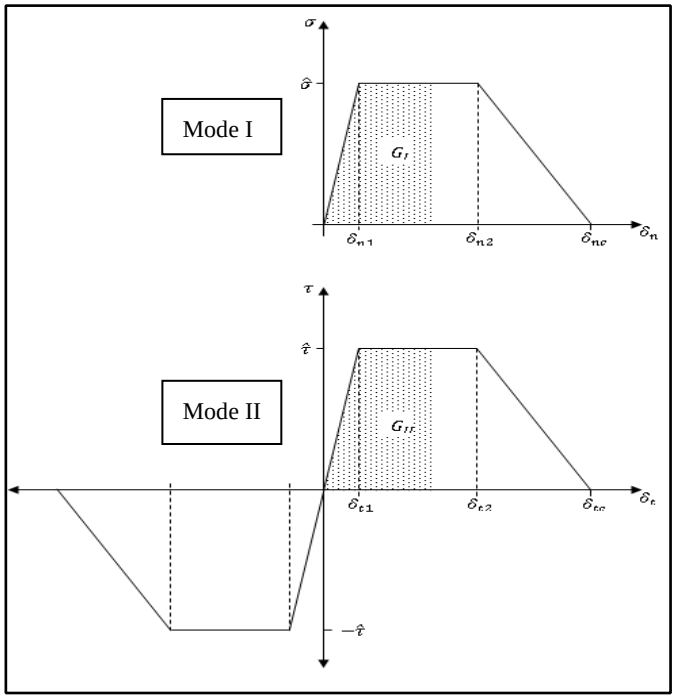

Figure 4: Traction-separation law for mode-I and mode-II fracture. The subscripts "n" and "t" denote the normal and shear directions respectively.

That is, as displacement increases, stiffness is degraded first at δ_1, then again at δ_2, until complete element failure occurs at δ_c. For this work, the ratios $^{\delta_1}/_{\delta_c}$ and $^{\delta_2}/_{\delta_c}$ were held at 0.01 and 0.75 respectively; varying these displacement ratios have a negligible effect on solutions. It is the cohesive strength and resulting toughness (area under the

curve) which control the behavior of fracture; fracture cannot occur unless these criteria are met. For displacements less than δ_c, the partial swept area under the curve is the instantaneous energy-release rate and when at δ_c, the total swept area is the toughness. The criterion for Mode-I fracture is therefore:

$$G_I/\Gamma_I = 1 \qquad (1)$$

and mixed-mode fracture occurs via a simple failure criterion:

$$G_I/\Gamma_I + G_{II}/\Gamma_{II} = 1 \qquad (2)$$

where $G$is the energy release rate, Γ is the material toughness, and subscripts I and II refer to Mode-I and Mode-II respectively. This failure criterion was chosen because of its success in work previously mentioned (Yang and Thouless [15], Kafkalidis and Thouless [16], and Li et al. [17]). Using the TSL as the governing constitutive relationship and the above failure criterion, the complete process of fracture can be modeled. Figure 5 illustrates how a TSL physically relates to the process of fracture. In Figure 5(a), each CZ sub-region is governed by an independent TSL. The left most

side of Figure 5(a) and Figure 5(b) correspond to a region which is completely unaffected by the fracture processes zone and is still exhibiting linear elastic behavior. The right-most side corresponds to a region that has completely fractured; critical displacement has been reached and all energy has been released. The region that lies in between no displacement and critical displacement is the process zone.

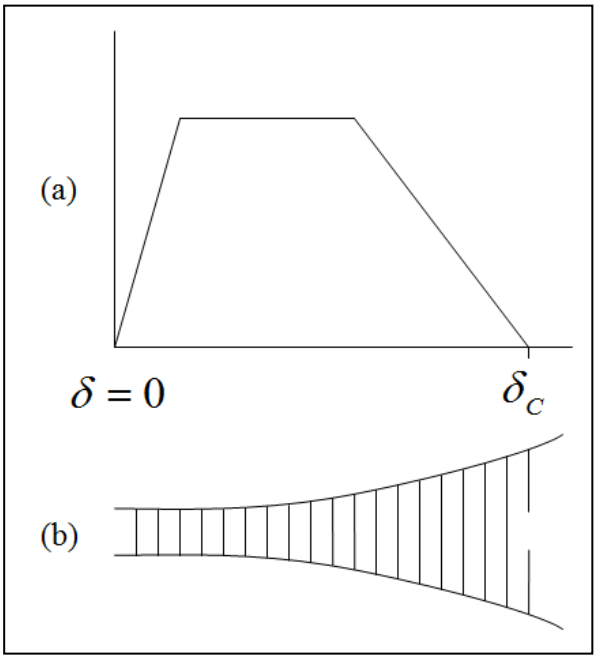

Figure 5: (a) The traction-separation law as it corresponds to (b) process of fracture.

The user therefore defines the fracture criterion for a CZ, by defining cohesive strength and toughness, cohesive strength and critical displacements, or toughness and critical displacements. In this work, crack growth in the penetrating direction is purely mode-I while crack growth in the deflecting direction is mixed-mode. The nonlinear

behavior of the above described traction-separation law can be defined and captured through the use of FEA.

Here, interface fracture is studied by means of a finite element model. The model consists of two bulk layers (referred to here as a film and substrate, and denoted by subscripts "f" and "s" respectively) separated by an interface layer (denoted by subscript the "i"). The film layer is cracked such that the crack is impinging upon the interface at a normal angle. A tensile load, $\sigma_{applied}$, is applied to the ends of the layered system as shown in Figure 6. Also, from Figure 6, see that the film and substrate layers are defined by their elastic modulus and Poisson's ratio. Further, all layers are isotropic and homogeneous. Under these circumstances, crack propagation can only penetrate through the interface and into the substrate or deflect along the interface. Finally, regions of cohesive elements are embedded in the deflecting direction (interface) and penetrating direction (substrate) and are defined by both cohesive strength and toughness properties.

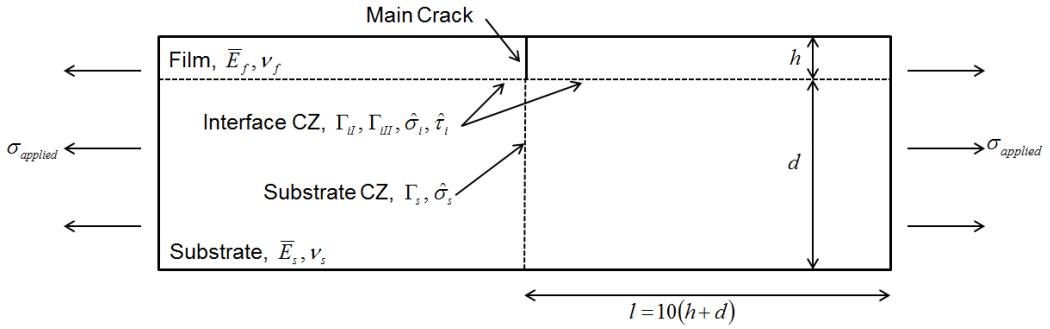

Figure 6: Model geometry and variables used CZ analyses. Dashed lines represent cohesive zones.

The finite element analyses performed for this work were executed using the commercial package ABAQUS (version 6.10). Using the ABAQUS user-defined element (UEL) feature, the constitutive relationship defined by the above described TSL and failure criterion was implemented through a custom FORTRAN subroutine. The UEL feature was used to define the elements which constructed the cohesive zones. These elements are therefore cohesive elements. This UEL can be found in Appendix A. It is identical to the UEL used in the work of Parmigiani and Thouless [10]. The remaining regions of the model (the film and substrate) were constructed using three and four node plane-stress continuum elements. In using plane-stress element formulation, the following definition for modulus of elasticity was used throughout:

$$\bar{E} = E \qquad (3)$$

In using this CZ formulation, two main sources of error were identified; one error is attributed numerical difficulties. Under some combinations of material properties, specifically those near transition conditions, it was found that the finite-element analysis failed to run until complete fracture occurred. That is, some analyses crashed before the failure criteria described by equations (1) and (2) was met. In the worst cases, analyses ran until only ~ 25% failure. In these instances, however, by simply shifting material properties slightly such that penetration was favored over deflection,

the analysis ran successfully until penetrating fracture occurred. Further, it was found that in the analyses that ran successfully, the relationship between the energy release rates in the penetrating and deflecting directions was linear. This principle was used to linearly extrapolate analyses which did not run until failure in order to confirm that simultaneous fracture had indeed occurred. The error associated with these extrapolations was calculated by examining slightly penetrating favored analyses which ran until complete failure. The error was found between a linear extrapolation (based on data from 25% fracture) and actual full fracture data. In the worst case, this error was found to be 8%. This worst case error is applied to data presented here in the form of error bars associated with critical strength and toughness ratios.

The second error in the CZ method used here is calculated based on analyzing a known simple fracture example and comparing it to its analytical solution. Here, a simple edge-cracked bar geometry is chosen for comparison; this geometry is appealing because it can be modeled by using the geometry described in Figure 6 and fixing any crack-tip-opening-displacement in the interface cohesive-zones (effectively removing the interface). The analytical solution used for comparison is from Tada et al. [18] and takes the form,

$$K_p = F\left({}^{h}/_{h+d}\right)\sigma_{applied}\sqrt{\pi h} \qquad (4)$$

where$K_p$is the stress intensity factor in the penetrating direction, h is the film thickness, d is the substrate thickness, $\sigma_{applied}$ is the applied axial load, and

$$F\left(h/h+d\right) = 0.265\left(1 - h/h+d\right)^4 + \frac{0.875 + 0.265\left(h/h+d\right)}{\left(1 - h/h+d\right)^{3/2}} \qquad (5)$$

Equation (4) can be rearranged to yield,

$$\sigma_{applied} = \frac{K_p}{F\left(h/h+d\right)\sqrt{\pi h}} \qquad (6)$$

Equation (6) is the applied load that would propagate fracture in the edge-cracked geometry. From Tada et al. [18], this formulation is accurate to 1%. When this problem was analyzed using the CZ method, a critical applied load was found with an associated 2.26% error with respect to the above analytical load. Further, the effect of error due to extrapolation (discussed in the previous paragraph) was examined. By forming a linear regression based on data up to 25% fracture and extrapolating the associated critical applied load, a maximum error of 3.82% was found. Note that this value is different than the 8% error stated above (applied to strength and toughness ratios) because the effect of the extrapolation is less pronounced on calculated

normalized fracture load. In total (summing these values), the error associated with the CZ method used here was found to be ~7%. This error is applied to data presented here in the form of error bars associated with the dimensionless group, $\sigma_{applied}\sqrt{\frac{h}{\bar{E}\Gamma_i}}$.

4.3 Dimensionless Groups

Dimensionless groups used in this study are introduced and described here. These dimensionless groups are the same as those used by Parmigiani and Thouless [10]. Using the Buckingham Pi Theorem, these dimensionless relationships were developed which completely define the cohesive-zone model. The length ratio, d/h, is simply the ratio between the substrate thickness and film thickness or crack-length. The substrate toughness-scale, $\frac{\Gamma_s}{\bar{E}_s h}$, is a value which compares the substrate toughness to substrate modulus while normalizing with respect to the crack-length. The physical interpretation of this dimensionless group is a relative toughness to stiffness ratio of the substrate. Next, the Dundurs parameters (as described by Dundurs [19]), $\alpha = \frac{\bar{E}_f - \bar{E}_s}{\bar{E}_f + \bar{E}_s}$, $\beta = \frac{1}{2}\left[\frac{\mu_f(1-2\nu_s)-\mu_s(1-2\nu_f)}{\mu_f(1-2\nu_s)+\mu_s(1-2\nu_f)}\right]$, depicts the relative stiffness and Poisson's effect of the film and substrate; this value controls the degree of mixed-mode behavior at the interface. The toughness ratio, Γ_s/Γ_i, is simply the ratio of substrate toughness to interface toughness. Similarly, the strength ratio, $\hat{\sigma}_s/\hat{\sigma}_i$, is the ratio of substrate

cohesive-strength to interface cohesive-strength. The fracture length-scale, $\frac{\bar{E}_f \Gamma_i}{\hat{\sigma}_i^2 h}$, $\frac{\bar{E}_s \Gamma_s}{\hat{\sigma}_s^2 h}$ (presented here for both the interface and substrate), is the dimensionless group which describes the length of the fracture process zone. That is, this value scales with the distance δ_c from Figure 5. Finally, the normalized fracture load, $\sigma_{applied}\sqrt{\frac{h}{\bar{E}\Gamma_i}}$, represents the applied load at which fracture begins.

5. Transition

As defined above, transition, refers to the changing from a case in which a main crack impinging upon an interface tends to penetrate to the case in which the crack tends to deflect (or vice versa). This occurrence has been studied by many using a variety of formulations, but has not been expressed as a specific event. Here, this unique event is a function of material and geometric properties which permits simultaneous crack growth in the penetrating and deflecting directions. That is, as load is applied to a cracked and layered geometry, like the one seen in Figure 6, stresses and energy release rates rise in both the penetrating and deflecting directions. Though not necessarily at the same rate, these values continue to rise until their associated critical values, be it a material toughness or a critical material strength, are reached. This fulfillment is reached at the exact same moment thus enabling simultaneous onset of fracture in both directions. This simultaneous growth and fracture occurs when the opportunity for propagation in the penetrating and deflecting directions is equal. In this section, transition is explored and discussed in great depth.

5.1 LEFM 3-Kink Approach

Here transition is examined using a three-kink approach and compared to previous formulations. The previous two-geometry approach used by He and Hutchinson [6] is correct in formulation, but does not reflect the characteristics of transition. As described above, at transition, crack growth occurs as penetration and deflection occur simultaneously. The two-geometry approach cannot capture this propagation behavior. To demonstrate this shortcoming, we consider a single, three-kink geometry, as shown in Figure 7. This geometry can be used to determine the energy release rate of kinks propagating in the penetrating and deflecting directions at the same time. Here, we use FEA to examine the three-kink geometry.

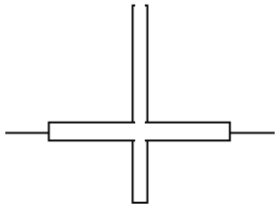

Figure 7: Three-kink geometry used to study penetration vs. deflection via LEFM formulation.

The method for performing an LEFM analysis using FEA is widely used and established; the collapsed-edge quarter point method was used. Using the FEA package ABAQUS (version 6.10) and referring to its documentation, ABAQUS Analysis User's Manual [20], a ring of eight node collapsed-edge quadrilateral elements (forming a ring of triangular elements) can be placed around the end of a pre-existing flaw. Further, each side node location is moved from a mid-point location to

a quarter-point location in order to properly take into account the $1/\sqrt{r}$ singularity present in LEFM formulations.

To analyze the problem of penetration versus deflection, an edge-cracked and axially loaded bar was analyzed. Per requirements of LEFM, pre-existing flaws (kinks) were placed at a main crack tip in the penetrating and deflecting directions. Figure 8 shows the geometry and properties used in the LEFM analyses in this work.

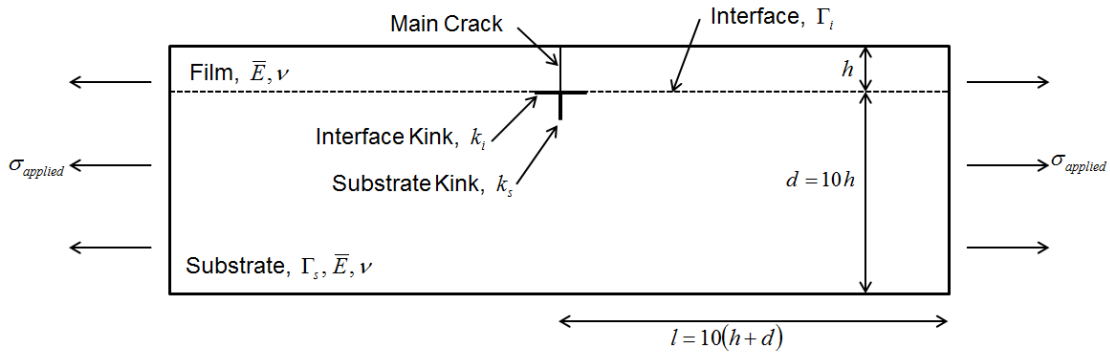

Figure 8: Model geometry and variables used in LEFM three-kink analyses.

Upon applying a remote axial stress, the stress intensity factors at the interface and substrate kinks were found and used to calculate the associated energy release rates using:

$$G_p = {K_p}^2 / \bar{E} \qquad (7)$$

and

$$G_d = {K_d}^2 \Big/ \bar{E} \qquad (8)$$

For a given applied load, $\sigma_{applied}$, failure was assumed to occur and thus the calculated ratio of energy release rates equates to a critical toughness ratio:

$$G_p \Big/ G_d = \Gamma_s \Big/ \Gamma_i \qquad (9)$$

This three-kink geometry was studied using a finite element model and method described above. It is worth noting that this method was applied to the two-kink geometry and the results of Figure 3 reproduced (see Figure 9) to within less than a 2% error.

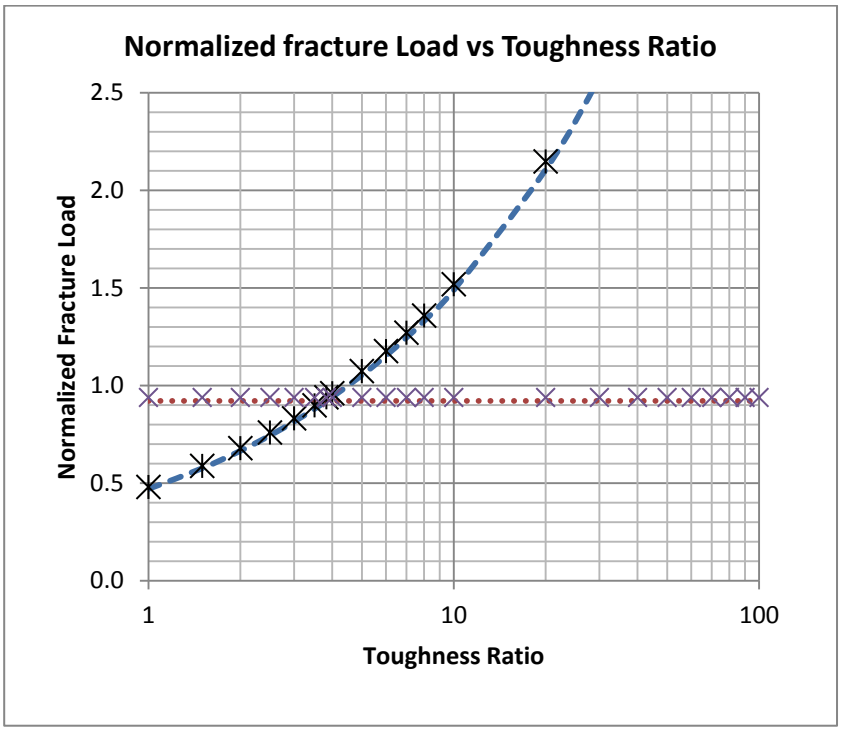

Figure 9: FEA LEFM analysis verified by comparing to LEFM two-geometry results.

The geometry of the model used in this three-kink analysis is shown above in Figure 8. This geometry includes interface and substrate kinks in the three-kink orientation and associated kink lengths, k_s and k_i. In this analysis, the relations $\frac{\Gamma_s}{\bar{E}h} = 10^{-6}$, $^{d}/_{h} = 10$, $^{d}/_{h} = 10$, and $k_s = k_i$ were kept constant. A convergence study was carried out to determine the appropriate kink length.

The relationship, $^{h}/_{k}$, which describes the relative thickness of the main crack length to the kink length, was used to control the kink length in a normalized fashion. For each analysis, the energy release rates in the penetrating and deflecting directions were observed and used to form the transition toughness ratio for that given geometry and dimensionless group combination. It was then assumed that toughness ratios less than that of the transition toughness ratio would result in penetration while toughness ratios greater than the transition toughness ration would result in deflection. Also, the normalized fracture load was calculated by extracting the applied force at which the energy release rates in the penetrating and deflecting directions reached their associated critical values. Starting with $^{h}/_{k} = 10$, the kink length was decreased until a toughness ratio was converged upon. The results of the study can be seen in Figure 10 and Figure 11. Figure 10 shows the resulting transition toughness ratios versus relative kink length. An asymptotic limit of $^{\Gamma_s}/_{\Gamma_i} = 9.8$ was found with reducing the kink length and convergence was found at $^{h}/_{k} = 10^5$. Similarly, Figure 11 shows the convergence of the normalized fracture load with respect to decreasing kink length.

Here, a limit of $\sigma_{applied}\sqrt{\frac{h}{\bar{E}\Gamma_i}} = 1.6$ was found. The resulting penetration/deflection curve can be seen in Figure 12; in this figure the normalized fracture load is plotted against toughness ratio for a range of kink lengths. Similar to the curves in Figure 3, the inflection point marks the point of transition from penetration to deflection. These results are supported by those presented by Wilson and Cherepko [21]. In this work, an investigation of stress intensity factors for multiple cracks branching at the end of a main-crack was carried out. The stress intensity factors yielded by the above three-kink analysis align with those found by Wilson and Cherepko [21].

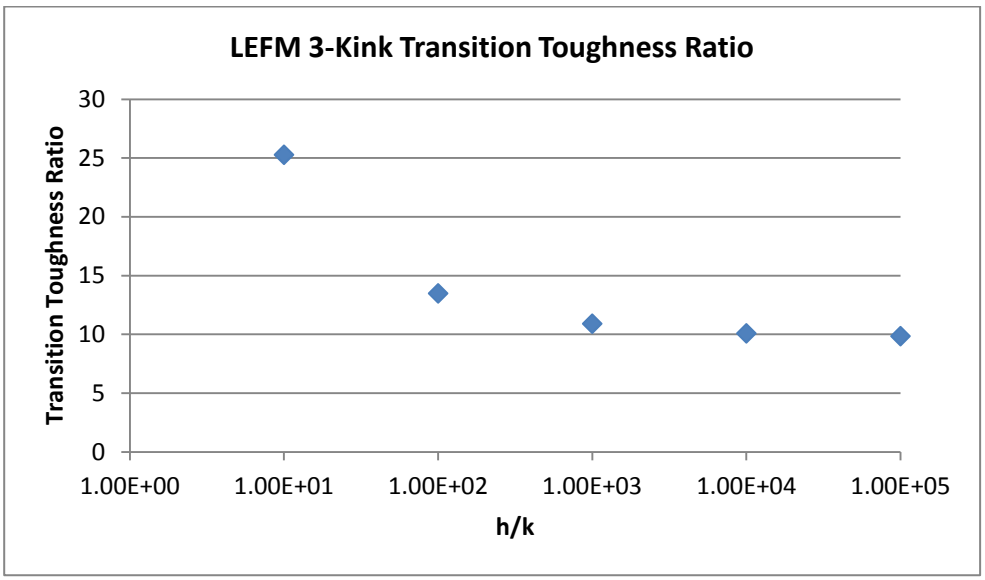

Figure 10: Three-kink solution; transition toughness ratio plotted against relative kink length.

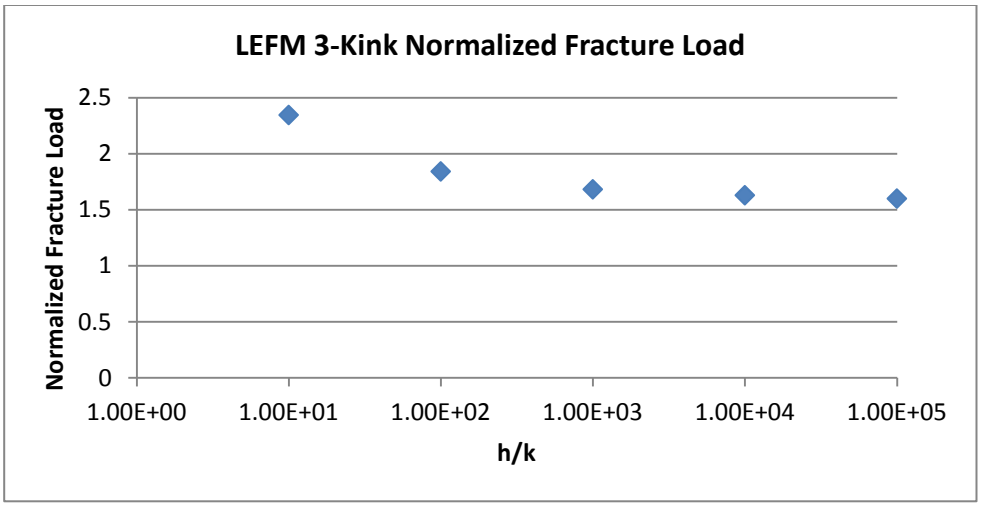

Figure 11: Three-kink solution; transition normalized fracture load plotted against relative kink length.

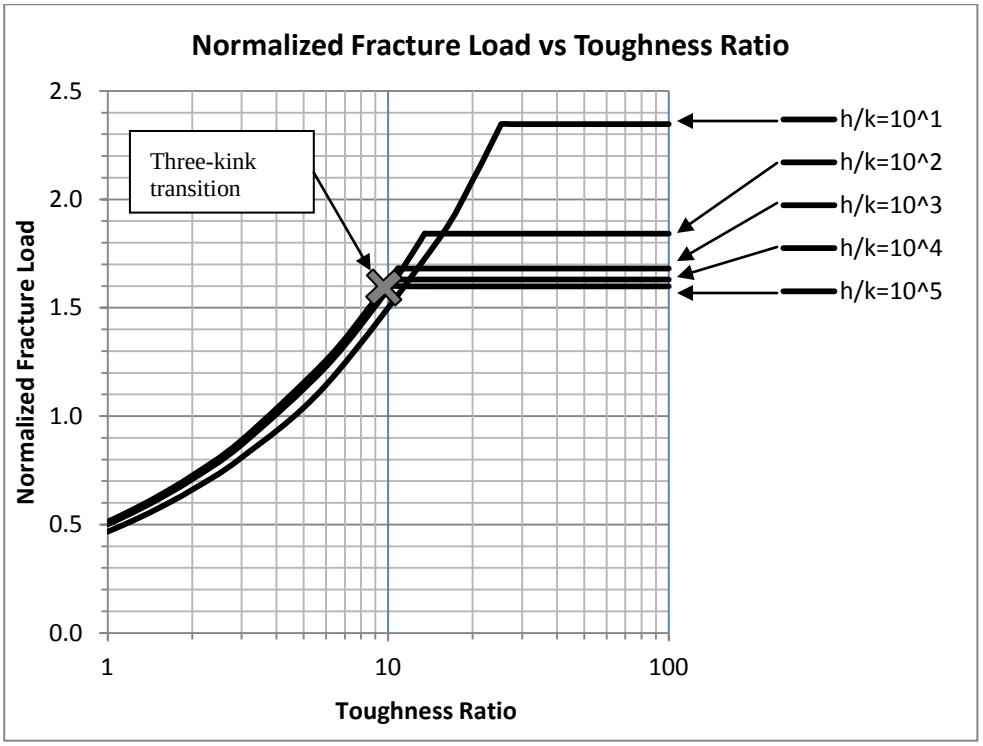

Figure 12: Three-kink solution; comparison of solutions among decreasing relative kink lengths.

There is a drastic difference between the He and Hutchinson [6] two-geometry solution and the above three-kink solution. Figure 13 shows these two solutions overlaid with each other. Most notably is the difference between the proposed toughness ratios and difference between normalized fracture loads. In terms of predicted transition toughness ratio, the two-geometry approach predicts ratio of $\Gamma_s/\Gamma_i \cong 4$ while the three-kink approach predicts a ratio of $\Gamma_s/\Gamma_i = 9.8$. This is a significant difference. Similarly, the two-geometry approach predicts a transition normalized fracture load of $\sigma_{applied}\sqrt{\frac{h}{\bar{E}\Gamma_i}} = 0.923$ while the three-kink approach predicts $\sigma_{applied}\sqrt{\frac{h}{\bar{E}\Gamma_i}} = 1.6$. Again, this is a significant difference. This significance of these differences is the fact that upon using one geometry versus the other a drastically different solution is derived. Based on these differences it is obvious that if the correct geometry is not analyzed, the correct solution may not be reached. In the next section, the geometry considered is further refined and analyzed using the CZ method.

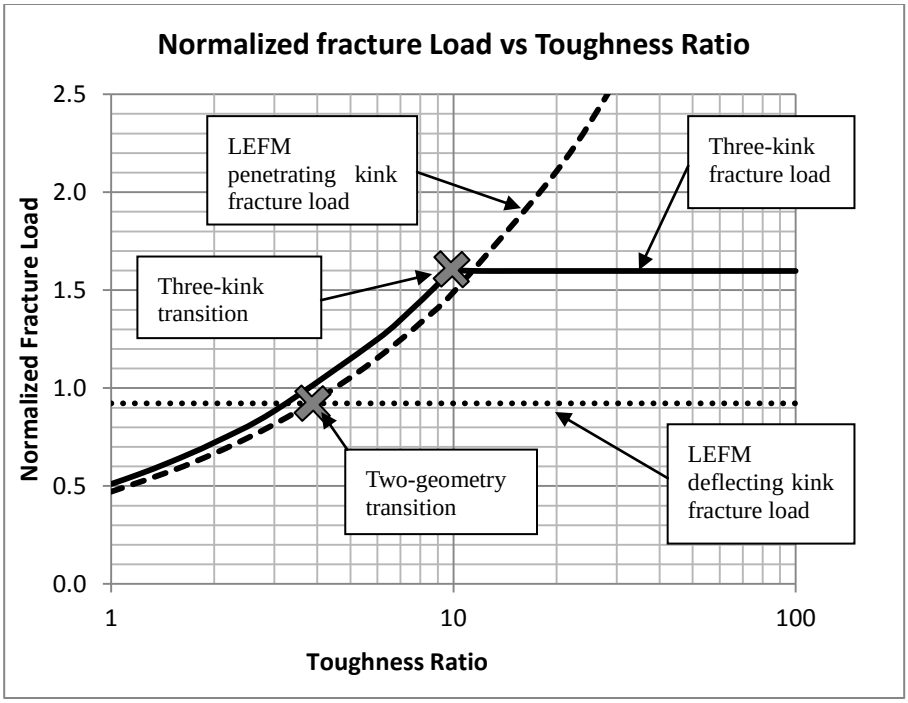

Figure 13: Comparison of He and Hutchinson [6] two-geometry solution and three-kink solution.

5.2 CZ Approach

Here, the CZ method described in section 4.2 is used to examine transition.

5.2.1 Behavior of Transition

A combined stress-energy-based approach is the most complete formulation because it does not exclude material strength or toughness and can be applied to the present problem without compromising the geometry. Previously discussed approaches are incomplete and/or compromise the modeling geometry due to requirements of the analysis. Both of the discussed stress-based approaches are incomplete in that they do not consider material toughness. The above discussed

energy-based approaches do not consider material strength and also used a modified geometry for analysis due the requirements of the LEFM formulation. In studying a main crack penetrating into the substrate or deflecting into the interface, the initial geometry should reflect that of a sharp notch impinging an interface as shown in Figure 14. The cohesive-zone method, as describe in the section 4.2 allows the proper geometry to be studied.

Figure 14: Geometry of sharp notch impinging interface used in cohesive modeling analysis.

Using the CZ method, a more accurate depiction of transition can be made. Figure 15 shows the process of fracture at the crack tip in a cracked bi-layer system (same model as described above by Figure 6) subject to conditions that promote transition. In this figure, cohesive elements are used to form penetrating and deflecting directions. The penetrating and deflecting cracks are the simultaneous extensions of the main crack. Further, simultaneous fracture occurs at transition when a critical amount of energy is released concurrently in the penetrating and deflecting direction.

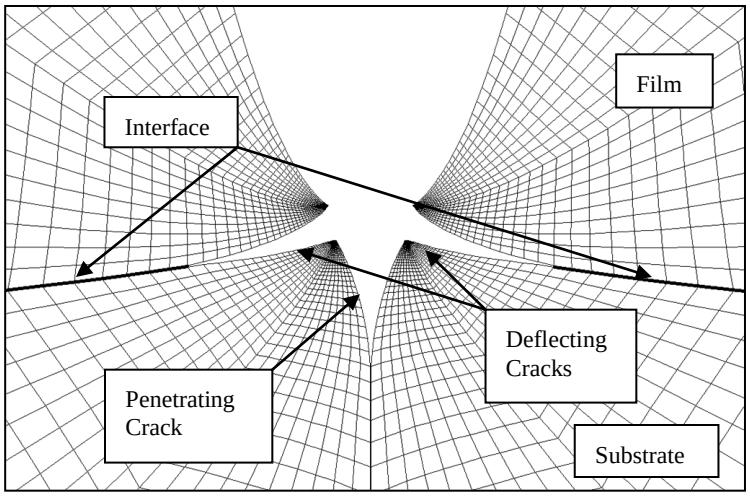

Figure 15: Finite element model illustration of simultaneous crack penetration and crack deflection.

With transition lying in the middle, the solution space between penetration and deflection is a continuum. Through the use of cohesive modeling, the entire spectrum between penetration and deflection can be examined; Figure 16 illustrates this spectrum. Using cohesive modeling, a range of material properties (from those which promote penetration to those which promote deflection) were solved for and illustrated in this figure. Previous formulations have been used to capture transition, but did so without considering the surrounding solution space. Transition has been characterized in the past using strength or energy methods.

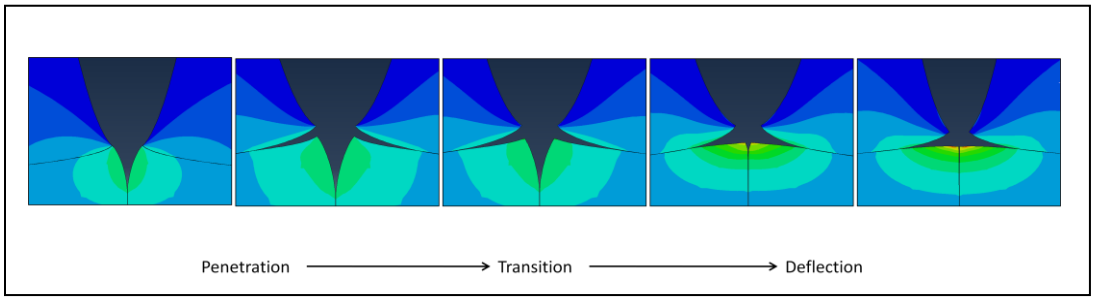

Figure 16: The transition continuum bounded by penetration and deflection.

The CZ method was used to quantitatively analyze the solution space surrounding transition. For a given set of dimensionless groups and a fully defined model, an analysis was carried out and the resulting fracture load was recorded. It was also noted what mode the fracture occurred in (penetration, deflection, or transition). The toughness ratio was then varied and the model was analyzed repeatedly. The solutions to this set of analyses form a curve similar to those in Figure 3 and Figure 12. Figure 17 shows the cohesive-zone analysis solution curve for ${}^{d}/_{h} = 10$, $\frac{\Gamma_s}{\bar{E}_s h} = 10^{-6}$, $\alpha = 0$, $\beta = 0$, $\frac{\bar{E}_f \Gamma_i}{\hat{\sigma}_i^2 h} = \frac{\bar{E}_s \Gamma_s}{\hat{\sigma}_s^2 h} = 10^{-5}$. The inflection point at ${}^{\Gamma_s}/_{\Gamma_i} = 7.4$ marks the critical transition toughness ratio. It is important to make clear that simultaneous crack propagation in the penetrating and deflecting directions occurs only at transition; to the left of the peak, the mode of fracture is penetration (though some energy is released in the deflecting direction, fracture occurs in the penetrating direction) and to the right is deflection (though some energy is released in the penetrating direction, fracture occurs in the deflecting directions). Also, the inflection point marks a peak normalized fracture load of $\sigma_{applied}\sqrt{\frac{h}{\bar{E}\Gamma_i}} = 1.5$. The shape of this curve is significant

because it indicates that a peak load carrying capacity exists at transition. This can be attributed to the dispersion of energy over multiple crack fronts; more energy can be absorbed by growing multiple cracks (simultaneous extension in both the penetrating and deflecting directions) than extending in either the penetrating or deflecting direction alone. Note that the energy-based, two-geometry approach fails to predict this intuitive result.

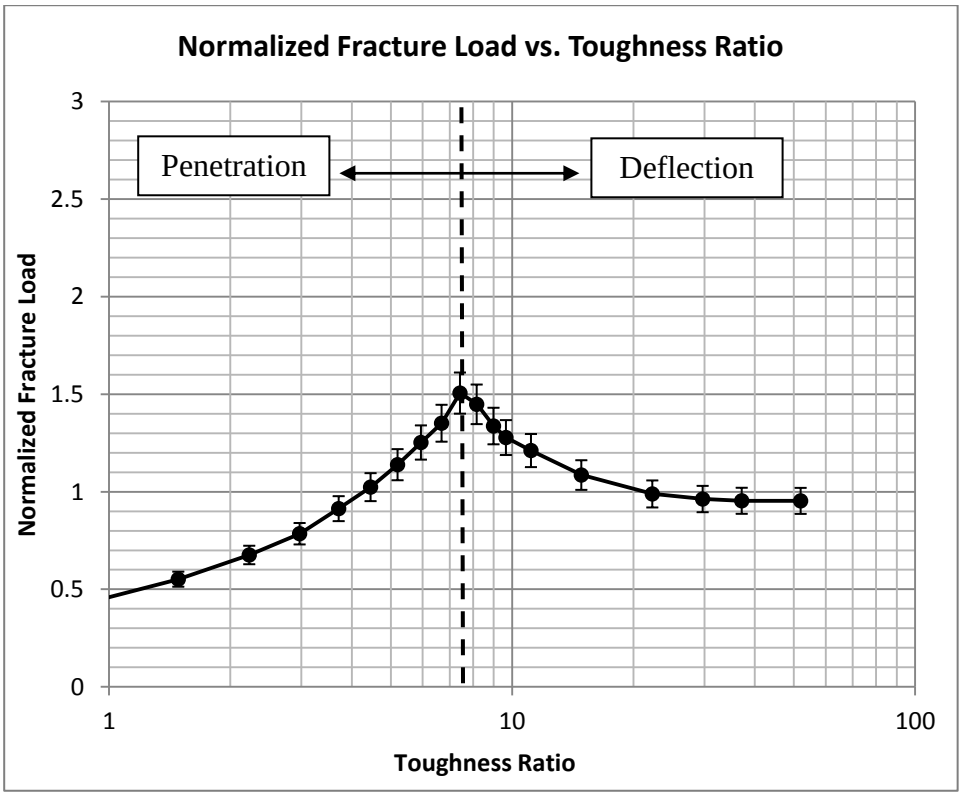

Figure 17: CZ solution shows peak like behavior at transition. The parameters $^{d}/_{h} = 10$, $\frac{\Gamma_s}{\bar{E}_s h} = 10^{-6}$, $\alpha = 0$, $\beta = 0$, $\frac{\bar{E}_f \Gamma_i}{\hat{\sigma}_i^2 h} = \frac{\bar{E}_s \Gamma_s}{\hat{\sigma}_s^2 h} = 10^{-5}$ were used.

At toughness ratios much greater or smaller than that of transition, the combined strength and energy approach aligns with the two-geometry solutions. At toughness

ratios much smaller than transition, substrate toughness is much less than interface toughness, which is similar to a geometry in which no interface crack is present. This corresponds to a kink in only the penetrating direction, which is one of the geometries of the two-geometry approach. Conversely, at toughness ratios much larger than that of transition, a geometry in which only deflecting cracks are present is emulated (corresponding to the other geometry of the two-geometry approach Figure 18 shows how the cohesive zone solution converges to the penetration-only and deflection-only solutions of the two-geometry approach. In this figure, the cohesive zone solution to the left of transition (small toughness ratios which favor penetration) converges to the penetrating only solution. Also, the cohesive zone solution to the right of transition (large toughness ratios which favor failure in the deflecting directions) converges upon the deflecting only solution. This occurs because far from transition, under the CZ approach large process zones form in either the penetrating or deflecting directions which behave similarly to the discrete kinks of the two-geometry model.

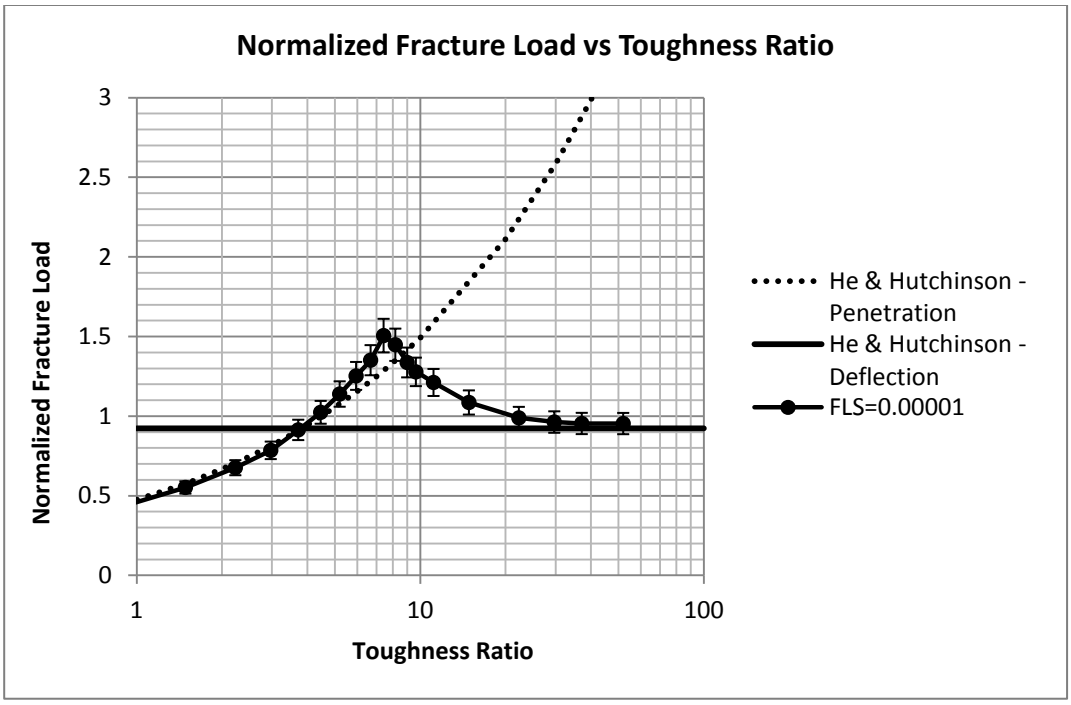

Figure 18: CZ solution predicts two geometry solution at very large and very small toughness ratios. Three-kink geometry used to study penetration vs. deflection via LEFM formulation. The parameters ${}^{d}/_{h} = 10$, $\frac{\Gamma_s}{\bar{E}_s h} = 10^{-6}$, $\alpha = 0$, $\beta = 0$, $\frac{\bar{E}_f \Gamma_i}{\hat{\sigma}_i^2 h} = \frac{\bar{E}_s \Gamma_s}{\hat{\sigma}_s^2 h} = 10^{-5}$ were used.

The approaches discussed in sections 3.1 and 3.2 fail to reveal the true nature of transition, giving the CZ method a significant insight to as how cracks act as they propagate simultaneously in the penetrating and deflecting directions. This is most apparent in comparing the CZ curve with the He and Hutchinson [6] two-geometry curves as the behavior of transition (the behavior between ${}^{\Gamma_s}/_{\Gamma_i} = 4$ and ${}^{\Gamma_s}/_{\Gamma_i} = 30$) goes completely un-captured by the latter approach. The impact of this difference is a region of increased load carrying capacity ($\sigma_{applied}\sqrt{\frac{h}{\bar{E}\Gamma_i}} = 1.5$ over $\sigma_{applied}\sqrt{\frac{h}{\bar{E}\Gamma_i}} =$

0.923, a 63% increase) which would have gone unseen if not for the presently applied CZ method.

5.2.2 Fracture Length-Scale

In this section, the effect of varying the fracture length-scale on transition is presented. As mentioned in section 4.3, the fracture length-scale is the dimensionless group which scales with the relative length of the process zone during fracture in cohesive-zone models (i.e. larger fracture length scales correspond to larger process zones). Small process zones are required for the LEFM method to be accurate.

The fracture length-scale has a great influence on transition. Using the cohesive modeling approach, a range of fracture length-scales were analyzed and compared. It is important to note that the fracture length-scales in the penetrating and deflecting directions were kept equal. In Figure 19, transition points are labeled, varied with fracture length-scale, and plotted against normalized fracture load. Further, the analytical LEFM solution for transition, developed in Appendix C as equation (29), is labeled and plotted on the same axes. As seen in the figure, the transition points for fracture length-scale at or below ~0.1, align with the analytical LEFM formulation. Alternatively, at fracture length-scales above ~0.1, the transition points begin to misalign and diverge rapidly from the LEFM solution. It is also important to notice that a peak is present at fracture length-scale ~1.

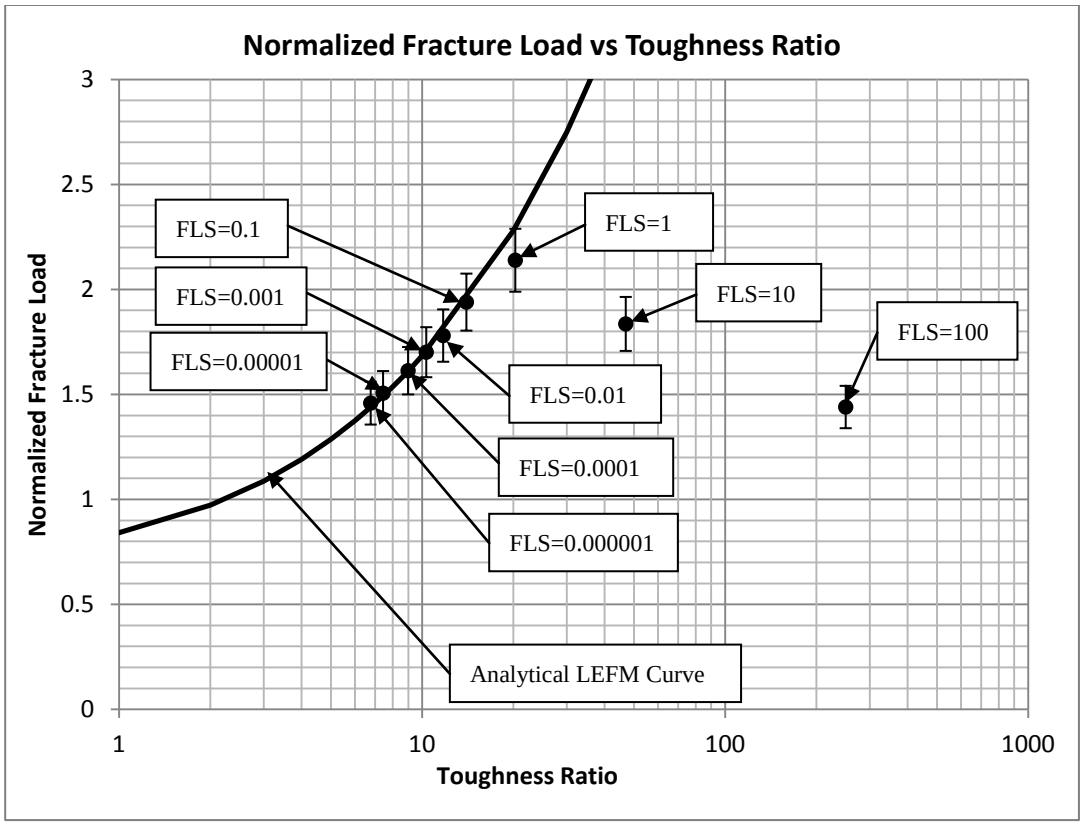

Figure 19: CZ transition points align with LEFM solution for decreasing fracture length-scales. The parameters $^{d}/_{h} = 10$, $\frac{\Gamma_s}{\bar{E}_s h} = 10^{-6}$, $\alpha = 0$, $\beta = 0$ were used.

At toughness ratios much less than the critical transition toughness ratio, solutions predicted using a wide variety of fracture length-scales converge to a common solution. The common solution is the penetration solution developed by He and Hutchinson [6]. Similarly, at toughness ratios much greater than the transition toughness ratio, the LEFM deflecting only solution is converged upon regardless of fracture length-scale has. Figure 20 shows this behavior; at both the low and high extremes, convergence is shared among varying fracture length scales. These

extremes converge to the two distinctly different geometry solutions developed by He and Hutchinson [6].

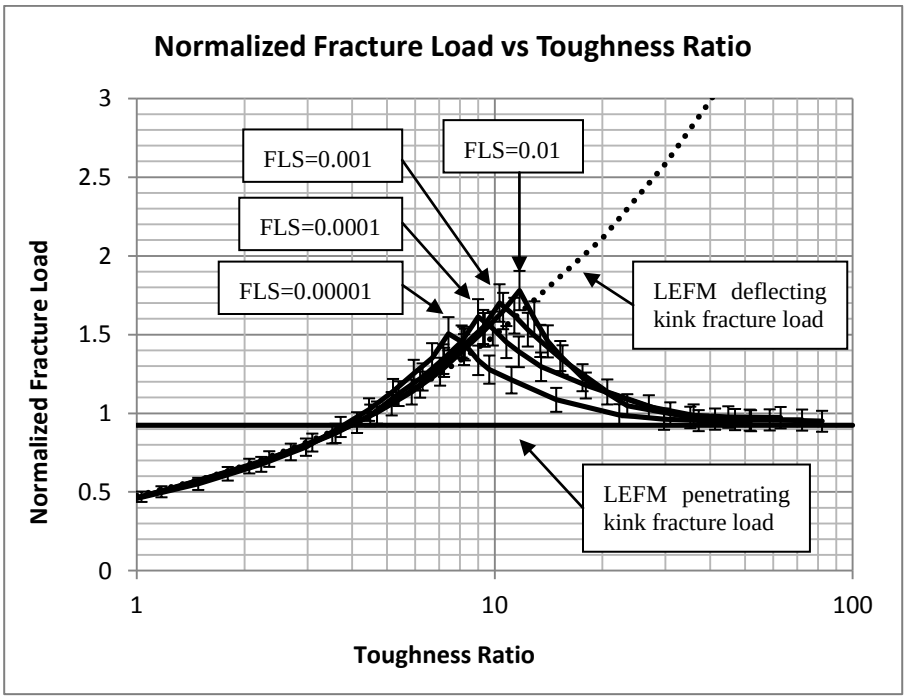

Figure 20: The effect of reducing the fracture length-scale on transition. The parameters $^{d}/_{h} = 10$, $\frac{\Gamma_s}{\bar{E}_s h} = 10^{-6}$, $\alpha = 0$, $\beta = 0$ were used.

Fracture length-scales can be varied independently of each other to provide curves that further define transition. Curves that distinguish between penetration and deflection can be formed by holding constant the interface fracture length-scale, systematically varying the substrate fracture length scale, and finding transition. Figure 21 shows one such transition curve; the interface fracture length-scale is held at 0.01 and the substrate fracture length-scale is varied from 0.0001 to 0.025. The curve represents the dividing line through penetrating and deflecting cases. This can easily

be understood by considering a point lying on the vertical portion of the curve; at substrate fracture length-scale greater than 0.1. From this point, decreasing the strength ratio, $\hat{\sigma}_s/\hat{\sigma}_i$, only would result in a material with a substrate strength that is decreasing with respect to the interface strength. A loaded system with relatively low substrate strength will penetrate. Alternately, increasing the strength ratio (traversing to the right side of the graph) will yield a system that will deflect. In this vertical region, toughness has little to no influence on penetration versus deflection. At lower substrate fracture length-scales (the more horizontal portion of the curve), however, both strength and toughness influence crack behavior. That is, from starting at a point on the transition cure, traversing horizontally (varying strength), vertically (varying toughness), or any combination of both strength and toughness will result in deviation from transition. Further, it is interesting to identify that for a substrate fracture length-scale approaching zero, the transition curve becomes horizontal (toughness dependent) and approaches horizontal asymptote at a toughness ratio of zero; the curve approaches a region in which penetration is impossible. The physical interpretation of this is a situation in which process zones exists in the deflecting directions and a relatively non-existent process zone in the penetrating direction; if no energy can be released in the penetrating direction, fracture is forced to occur in the deflecting directions.

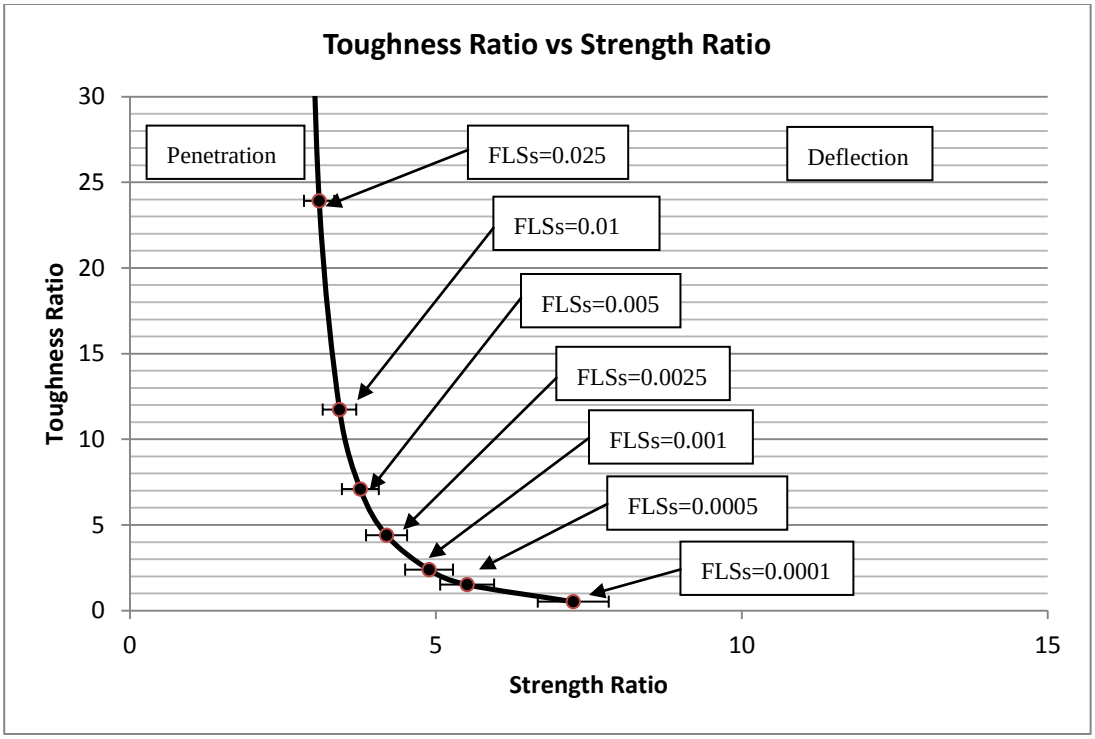

Figure 21: Transition curve. The parameters $^{d}/_{h} = 10$, $\frac{\Gamma_s}{\bar{E}_s h} = 10^{-6}$, $\alpha = 0$, $\beta = 0$, $\frac{\bar{E}_f \Gamma_i}{\hat{\sigma}_i^2 h} = 10^{-2}$ were used.

Here, it is useful to make a comparison to the stress-based solution developed by Gupta et al [5]; this transition criteria can be seen in Figure 22. The line, defined by $^{\sigma_s}/_{\sigma_i}\big|_{transition} \approx 3$ represents the dividing criteria between a penetrating case and a deflecting case. Further, in Figure 23, the transition strength ratio developed by Gupta et. al [5] is shown as a dashed vertical line. For this interface fracture length-scale, the transition curve seems to converge to the proposed $^{\sigma_s}/_{\sigma_i}\big|_{transition} \approx 3$ indicating that this solution is valid for this set of material properties.

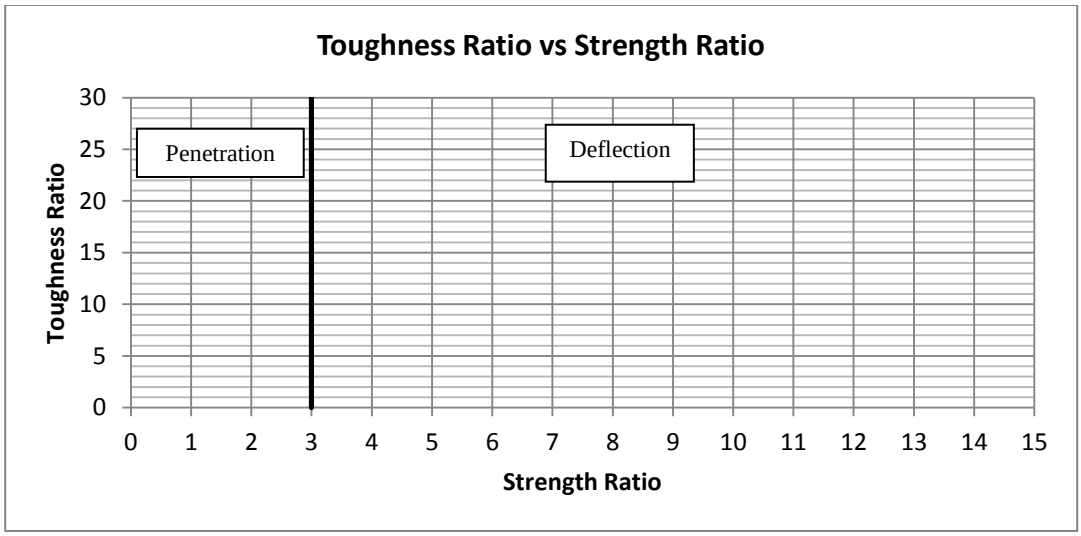

Figure 22: The Gupta et. Al [5] stress-based solution for determining transition does not consider any aspect of material toughness.

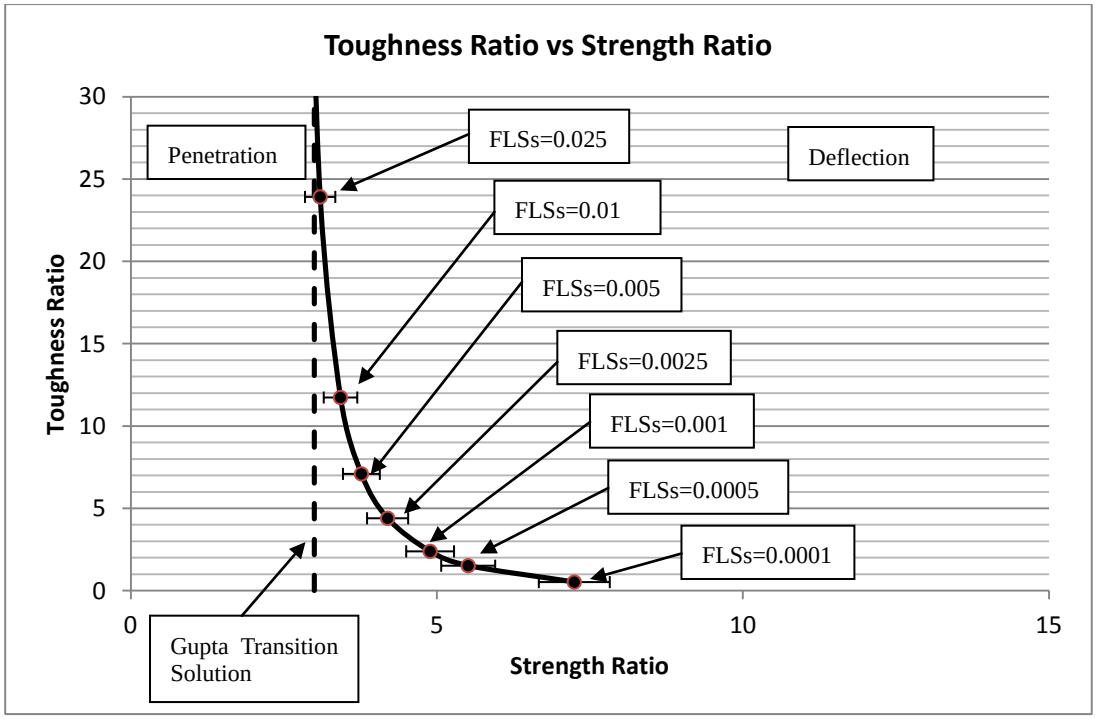

Figure 23: Transition curve. The Gupta et. al [5] strength ratio of ~3 is shown as a vertical dashed line. The parameters for $^{d}/_{h} = 10$, $\frac{\Gamma_s}{\bar{E}_s h} = 10^{-6}$, $\alpha = 0$, $\beta = 0$, $\frac{\bar{E}_f \Gamma_i}{\bar{\sigma}_i^2 h} = 10^{-2}$ were used.

When transition curves for multiple interface fracture length scales are plotted beside each other on the same axes, an interesting trend emerges. Figure 24 shows a range of such transition curves. Each curve shown here exhibits the same general shape as that in Figure 23; the major distinguishing element is a translated position. Starting with the rightmost curve, $\frac{\bar{E}_f \Gamma_i}{\hat{\sigma}_i^2 h} = 100$, each curve to the left is defined by a decreasing interface fracture length-scale. The leftmost curve has an interface fracture length-scale of $\frac{\bar{E}_f \Gamma_i}{\hat{\sigma}_i^2 h} = 10^{-5}$. Furthermore, each subsequent curve with decreasing FLSi are spaced closer together indicating some limit is being approached. In examining the transition strength ratio proposed by Gupta et al. [5] in comparison with the rest of the transition curves, as seen in Figure 24, it appears as though the critical strength ratio of $\sigma_s/\sigma_i\big|_{transition} \approx 3$ is in close proximity to the vertical portions of transition curves for 0.0001<FLSi<0.1. This indicates this previous solution is valid for this range of material properties.

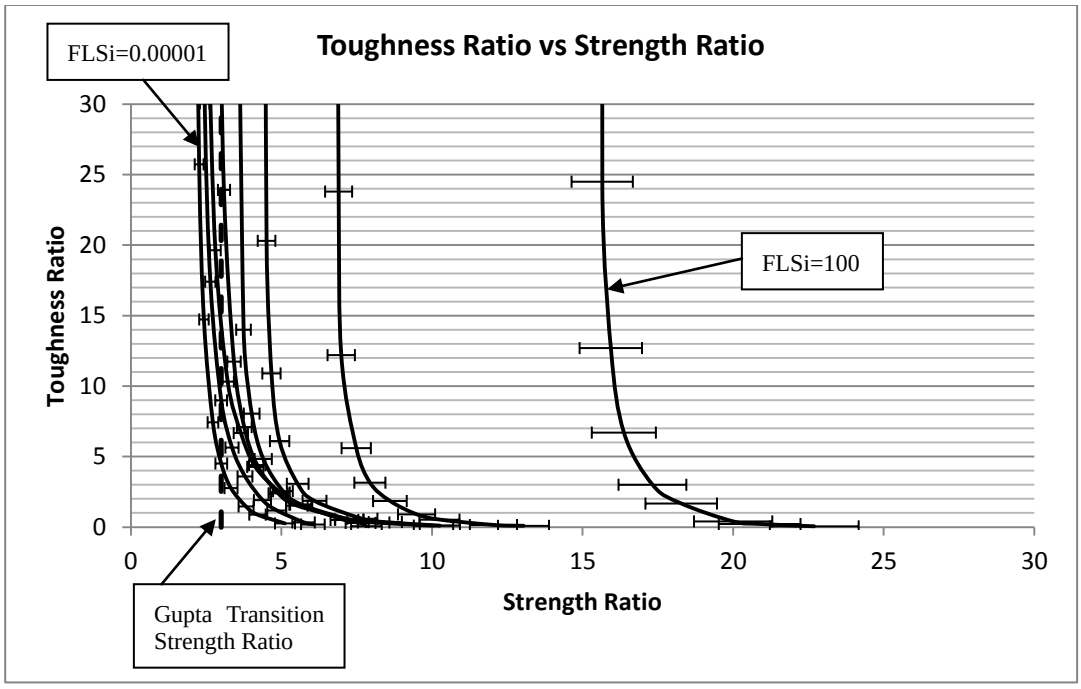

Figure 24: Transition curves for decreasing fracture length-scale. The leftmost curve is for $\frac{\bar{E}_f \Gamma_i}{\hat{\sigma}_i^2 h} = 10^{-5}$ and the rightmost curve is for $\frac{\bar{E}_f \Gamma_i}{\hat{\sigma}_i^2 h} = 100$; intermediate curves are separated by factors of $\frac{\bar{E}_f \Gamma_i}{\hat{\sigma}_i^2 h} =$ 10X. The Gupta et. al [5] strength ratio of ~3 is shown as a vertical dashed line. The parameters $d/h = 10$, $\frac{\Gamma_s}{\bar{E}_s h} = 10^{-6}$, $\alpha = 0$, $\beta = 0$ were used.

This apparent limit can better be examined by plotting the critical transition toughness and strength ratios against their respective fracture length-scales. If a limit exists, a horizontal limit will exist at some strength or toughness ratio. In Figure 25, transition strength and toughness ratios are plotted against their corresponding fracture length-scales (equal for interface and substrate). The shape of the curve defined by toughness ratios and the curve defined by strength ratios are very similar in shape; this is to be expected as the transition toughness ratios are defined to be the square of the transition strength ratios for any given fracture length-scale. From the rightmost side

of the plot (fracture length-scale equal to 100, transition strength and toughness ratios seem to converge rapidly with decreasing fracture length-scale. This is the same behavior displayed in Figure 24. See also, in Figure 25, that the Gupta et. Al [5] strength ratio of $\sigma_s/\sigma_i\big|_{transition} \approx 3$ is shown as a horizontal line. As fracture length-scale continues to decrease (less that ~0.01), however, it appears as though transition strength and toughness ratios decrease slightly in a linear manner and no asymptotic limit exists. This may be explained in that a finite process zone length is required for fracture so a self-similar situation is never created.

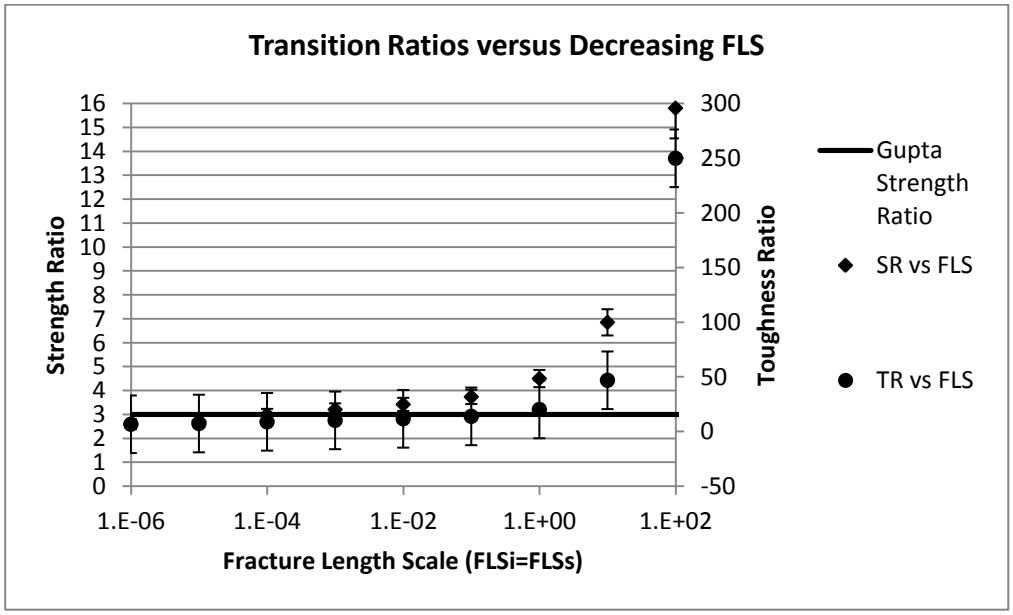

Figure 25: Transition strength and toughness ratios decrease with fracture length-scale.

5.3.3 Substrate Toughness-Scale

Here, the effect of varying the substrate toughness-scale is examined. Recall that this dimensionless group quantifies the substrate toughness with respect to the

substrate modulus and normalizes by the main crack-length. In all previously shown analyses, this dimensionless group was held at 10^{-6}. Figure 26 shows the effect of varying the substrate toughness-scale on transition toughness ratio for fracture length-scale of 0.001 (the most computationally stable fracture length-scale studied). It is apparent that a horizontal limit is met with decreasing substrate toughness-scale. That is, as the substrate toughness-scale is decreased (below 10^{-7}) and the transition toughness ratio is found, the toughness ratio reaches an upper limit of ~11.

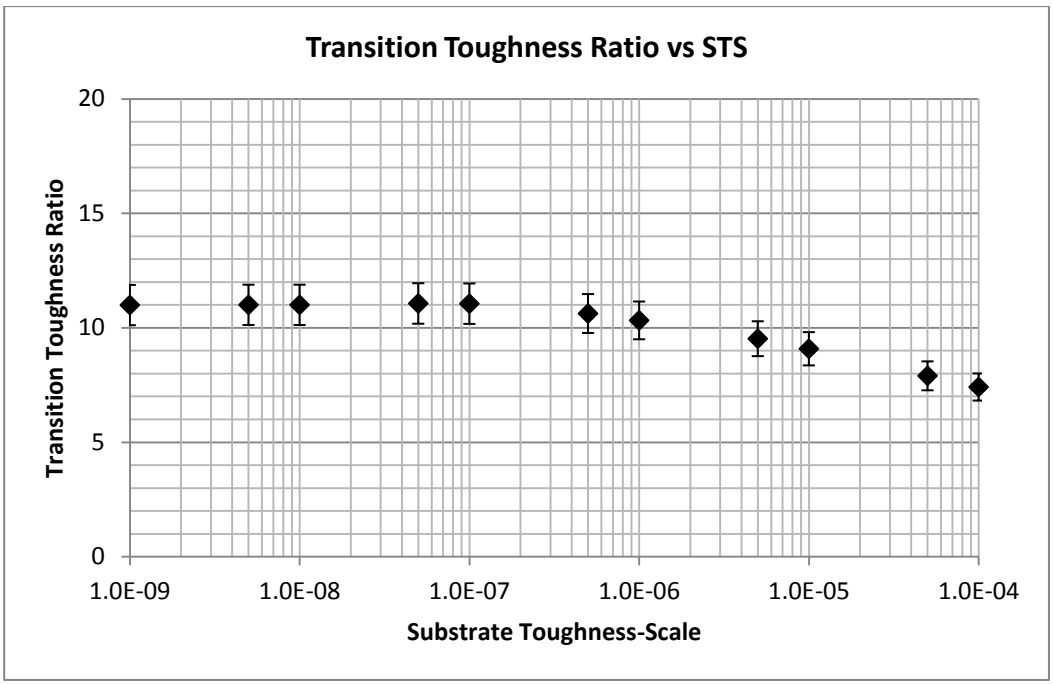

Figure 26: Transition toughness ratio plotted against substrate toughness-scale. The parameters $^{d}/_{h} = 10$, $\alpha = 0$, $\beta = 0$, $\frac{\bar{E}_f \Gamma_i}{\hat{\sigma}_i^2 h} = \frac{\bar{E}_s \Gamma_s}{\hat{\sigma}_s^2 h} = 10^{-3}$ were used.

5.2.3 Dundurs Parameters

In this section, the effect of varying the Dundars parameter, α, is examined. In all previously discussed results, this dimensionless value (along with the other commonly used Dundurs parameter, β) was held at zero. Here $\alpha = \frac{\bar{E}_f - \bar{E}_s}{\bar{E}_f + \bar{E}_s}$ is varied. The physical interpretation of this is a relative elastic modulus mismatch between the film and substrate. The range of possible values for α exist between the limits -1 and 1; the limits represent cases which one material has infinitely greater elastic modulus than the other. It is important to note however, for real materials and holding β=0, realistic values for α exist near $\alpha = 0$. It is accepted, however, that for results like those presented here, that the range of $-1 < \alpha < 1$ for $\beta = 0$ be presented. In this work, when $\alpha = -1$, the elastic modulus of the substrate is infinitely greater than that of the film. Alternately, when $\alpha = 1$, the elastic modulus of the film is infinitely greater than that of the substrate.

The effect of varying α on the normalized fracture-load shows extreme behavior. Figure 27 shows the effect of varying α between its limits on the transitional normalized fracture-load. As α approaches -1, the associated transitional normalized fracture-load goes to infinity. This can be attributed to the extreme stiffness of the substrate relative to the film; to reach transition at this infinite mismatch, an infinite normalized fracture-load is required. Conversely, as α approaches 1, the opposite occurs and an infinitely small normalized-fracture load is required to propagate fracture in both the penetrating and deflecting directions.

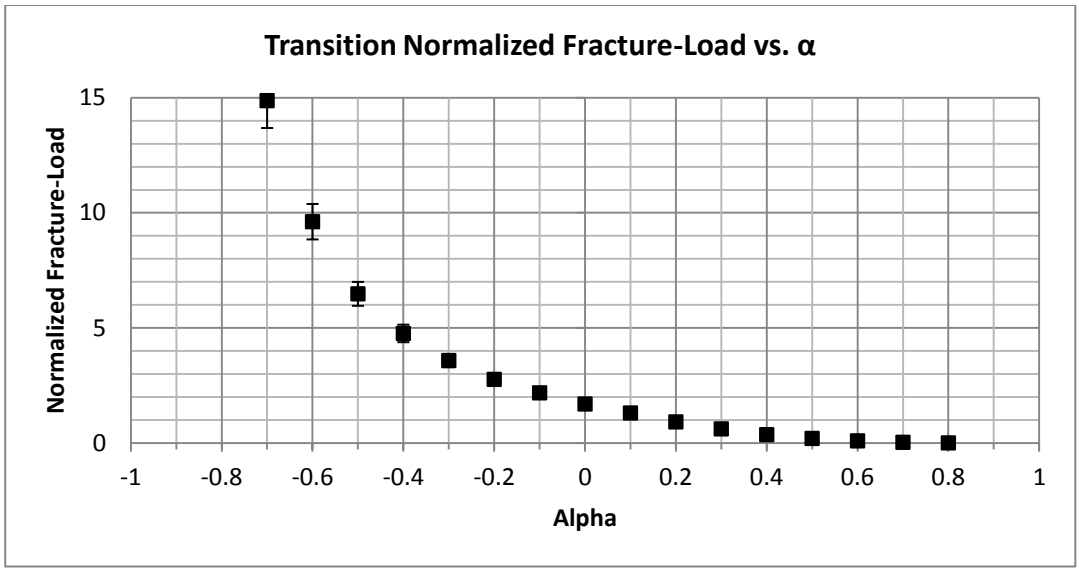

Figure 27: Normalized fracture-load plotted against the Dundurs parameter alpha. The parameters $d/h = 10$, $\frac{\Gamma_s}{\bar{E}_s h} = 10^{-6}$, $\beta = 0$, $\frac{\bar{E}_f \Gamma_i}{\bar{\sigma}_i^2 h} = \frac{\bar{E}_s \Gamma_s}{\bar{\sigma}_s^2 h} = 10^{-3}$ were used.

The end behavior of the transition toughness ratio curve is less extreme. Figure 28 shows the effect of varying α between its limits on the transition toughness ratio. A distinct maximum toughness ratio occurs at approximately $\alpha = 0.3$. This equates to a film elastic modulus that is ~1.86 times greater than that of the substrate. The significance of a maximum transition toughness ratio (here the maximum is ~14) is a region of opportunity for penetration. On either side of this peak are areas of decreasing toughness ratios until apparent end convergence at toughness ratios of ~2 and ~6 at α values of -1 and 1 respectively. These areas of decreasing toughness ratio are indicative of areas of increased opportunity for deflection. A valid use of the data presented in Figure 27 and Figure 28 is in designing a relatively strong bi-layer material system that favors deflection; if a material was designed to have an α value of

less than zero, it will be relatively stronger and have an increased likelihood of deflection than a system having an α value of greater than zero.

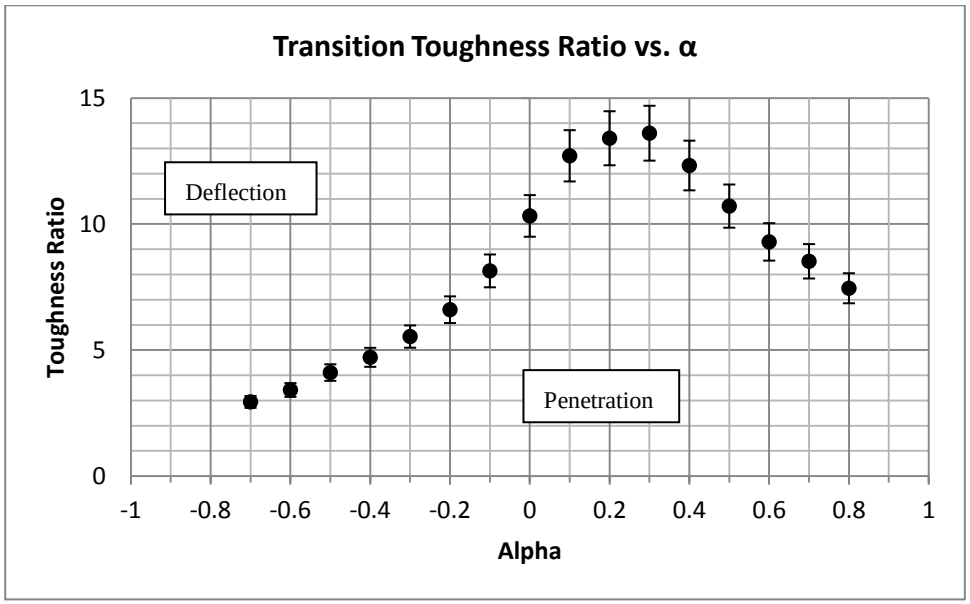

Figure 28: Transition toughness ratio plotted against the Dundurs parameter alpha. The parameters $d/h = 10$, $\frac{\Gamma_s}{\bar{E}_s h} = 10^{-6}$, $\beta = 0$, $\frac{\bar{E}_f \Gamma_i}{\bar{\sigma}_i^2 h} = \frac{\bar{E}_s \Gamma_s}{\bar{\sigma}_s^2 h} = 10^{-3}$ were used.

5.2.4 Linear vs. Nonlinear Geometry

In this section, the effect of using the nonlinear solving algorithm built into ABAQUS is discussed. In all previously discussed analyses, solutions were found using a linear solving method. In linear solving methods, the stiffness matrix is formed and solved once for an entire analysis. This solution method assumes that stiffness properties of the system are constant throughout the analysis. It is important to note that the material nonlinearities that are present throughout the process of fracture are handled separately from the solver by the UEL. By using a nonlinear

solution method, the ABAQUS solver forms and solves the finite-element model's stiffness matrix for each iteration. By doing this, non-linear problems, such as large displacement problems where tractions become misaligned as the model deforms, can be solved.

When the nonlinear solution method was applied to the problem at hand, alternate solutions were found. Figure 29 shows the difference among transition points between linear and nonlinear solutions against the analytical LEFM curve. Recall, from Figure 19, that the linear solution converges to the analytical LEFM curve. From Figure 29, however, it is clear that the nonlinear solution diverges from the analytical LEFM solution at small fracture length scales (FLS<0.1). It makes sense that the linear solution method converges with the analytical LEFM solution since both are linearly derived. It is unclear, however, why the nonlinear solution differs so drastically at small fracture length scales. In examining the problem studied here, it does not seem as though a nonlinear solution method should converge to a different solution set than the linear solution method. Further, it is unclear which solution set is more valid. Examining the use of nonlinear solution methods in combination with the combined strength and energy approach, presented here, should be pursued and further investigated.

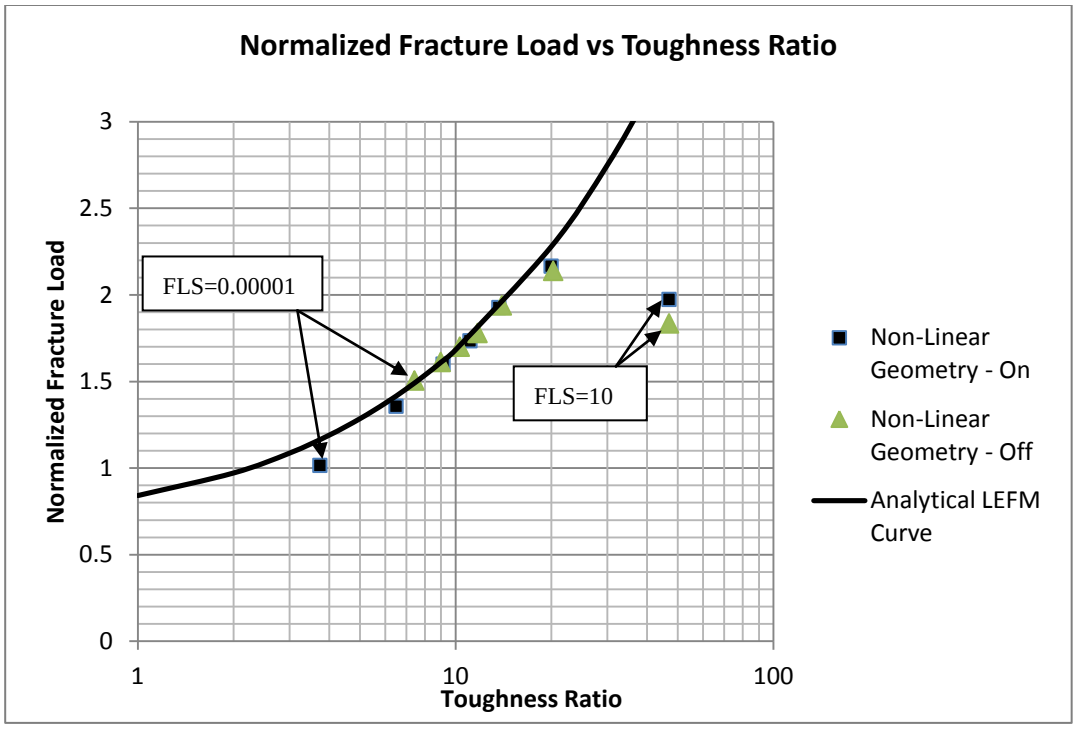

Figure 29: The use of the non-linear geometry results in a different solution than those not considering non-linear geometry. The parameters $^{d}/_{h} = 10$, $\frac{\Gamma_s}{\bar{E}_s h} = 10^{-6}$, $\alpha = 0$, and $\beta = 0$ were used.

6. Conclusion

Many formulations have been developed to determine the behavior of a crack impinging normally upon an interface using stress-based and energy-based approaches. One main contribution of these analyses has typically been some critical substrate-interface strength or toughness ratio which acts as the distinguishing value between crack penetration (into the substrate) and deflection (along the interface). Though these formulations were not derived with transition (as described in present work) in mind, these critical ratios do indicate combinations of material proerties which should permit simultaneous fracture in the penetrating and deflecting directions;

transition. In reviewing previous work, an obvious disconnect among approaches is that some are stress-based and some are energy-based formulations. The disconnect is that in considering only one metric (material strength or toughness) the complimentary property is disregarded. Present work, in using a combined stress-energy-based approach (a cohesive-zone method), shows the entire spectrum of transition solutions including those derived with stress-based and energy-based formulations. That is to say the strength-energy-based solution acts as a connection between previous work, showing under what circumstances a given formulation is valid or not valid. In comparing to both the CZ forumlation and a computational LEFM formulation. it was found that one popular solution for penetration versus deflection, the work of He and Hutchinson [6], does not appropriately predict transition. This inaccuracy is due to incorrectly applied two-geometry approach. This formulation, however, does seem to produce an accurate solution for a deflecting only or penetrating only geometry. Alternately, it was shown that the transition strength ratio proposed by Gupta et al. [5] may be valid in for geometries in which interface fracture length-scale is in the range $0.0001<FLSi<0.1$ and the substrate interface fracture length-scale is greater than that of the interface fracture length-scale.

Using the CZ approach, transition was also investigated in a general manner by varying a collection of dimensionless groups. It is shown that for small fracture length-scales (at or below ~0.1), the CZ solution aligns with that predicted by LEFM, an energy-based solution. This alignment is shown between an analytically derived LEFM solution for present geometry and the CZ analysis for varying fracture length-

scales. The effect of varying of dimensionless groups, including the substrate toughness-scale and the Dundurs parameter α, is also examined. It was concluded that for substrate toughness-scales below 10^{-7}, this dimensionless group has no effect on the transition toughness-ratio. Further, it was found that a region of maximized opportunity for penetration exists for $\alpha \approx 3$.

Finally, two recommendations are made for future work. First, it is recommended that further refinement of the finite element model used in present work be pursued in future work. Numerical instabilities and limits were introduced in this work due to the mesh refinement necessary to study small fracture length-scales. These limitations directly inhibited pursuing fracture length-scales $< 10^{-5}$. In being able to analyze said smaller fracture length-scales, a higher degree of confidence could be had in postulating possible asymptotic limits. Specifically, in examining the data in Figure 25; the end behavior (as fracture length-scale decreases) does not yield any definite or indefinite convergence. Second, it is recommended that the UEL used to deploy the CZ method, or the method in which the UEL interacts with the rest of the finite element model, be enhanced to include a higher degree of stability. One major difficulty encountered in the work presented here was building a finite element analysis that would run until the CZ would fracture. This was especially apparent in analyses which portrayed transitional behavior. Elemental stability methods, such as damping, should be pursued in order achieve a robust analysis.

7. References

[1] M. Ruhle, B. J. Dalgeish and A. G. Evans, "On the toughening of ceramics by whiskers," *Scripta Metallurgica* , vol. 21, no. 5, pp. 681-686, 1987.

[2] G. H. Cambell, M. Ruehle, B. J. Dalglesh and A. G. Evans, "Whisker Toughening: A Comparison Between Aluminum Oxide and Silicon Nitride Toughened with Silicon Carbide," *Journal of the American Ceramic Society,* vol. 73, no. 3, pp. 521-530, 1990.

[3] K. T. Faber and A. G. Evans, "Crack deflection processes—I. Theory," *Acta Metallurgica,* vol. 31, no. 4, pp. 565-576, 1983.

[4] J. Cook, J. E. Gordan, C. C. Evans and D. M. Marsh, "A Mechanism for the Control of Crack Propagation in All-Brittle Systems," in *Proceedings of the Royal Society of London. Series A, Mathematical and Physical Sciences,* London, 1964.

[5] V. Gupta, A. Argon and Z. Suo, "Crack Deflection at an Interface Between Two Orthotropic Media," *Journal of Applied Mechanics,* vol. 59, pp. 79-87, June 1992.

[6] M.-Y. He and J. W. Hutchinson, "Crack Deflection at an Interface Between Disimilar Materials," *Int. J. Solids Structures,* vol. 25, pp. 1053-1067, 1989.

[7] E. Martin, D. Leguillon and C. Lacroix, "A revisited criterion for crack deflection at an interface in a brittle bimaterial," *Composites Science and Technology,* vol. 61, pp. 1671-1679, 2001.

[8] D. L. Tullock, I. E. Reimanis, A. L. Graham and J. J. Petrovic, "Deflection and Penetration of Cracks at an Interface Between Two Dissimilar Materials," *Acta Metallurgica et Materialia,* vol. 42, no. 9, pp. 3245-3252, 1994.

[9] D. Martinez and V. Gupta, "Energy Criterion for Crack Deflection at an Interface Between Two Orthotropic Media," *J. Mech. Phys. Solids,* vol. 42, pp. 1247-1271, 1994.

[10] J. P. Parmigiani and M. Thouless, "The roles of toughness and cohesive strength on crack deflection at interfaces," *Journal of the Mechanics and Physics of Solids,* vol. 54, pp. 266-287, 2006.

[11] E. Martin, B. Poitou, D. Leguillon and J. M. Gatt, "Competition between deflection and penetration at an interface in the vicinity of a main crack," *International Journal of Fracture,* vol. 151, pp. 247-268, 2008.

[12] D. Leguillon, "Strength or toughness? A criterion for crack onset at a notch," *European Journal of Mechanics A/Solids,* pp. 61-72, 2002.

[13] D. S. Dugdale, "Yielding of Stel Sheets Containing Slits," *J. Mech. Phys. Solids,* vol. 8, pp. 100-104, 1960.

[14] G. I. Barenblatt, "The Mathematical Theory of Equilibrium Cracks in Brittle Fracture," *Advances in Applied Mechanics,* vol. 7, pp. 55-129, 1962.

[15] Q. D. Yang and M. D. Thouless, "Mixed-mode fracture analyses of plastically-deforming adhesive joints," *Int. J. Fract.,* vol. 110, pp. 175-187, 2001.

[16] M. S. Kafkalidis and M. D. Thouless, "The effects of geometry and material properties on the fracture of single," *J. Solids Struct.,* vol. 39, pp. 4367-4383, 2002.

[17] S. Li, M. D. Thouless, A. M. Waas, J. A. Schroeder and P. D. Zavattieri, "Mixed-mode cohesive-zone models for fracture of an adhesively-bonded polymer-matrix composite," *J. Eng. Fract. Mech.,* vol. 73, pp. 64-78, 2006.

[18] H. Tada, P. C. Paris and G. R. Irwin, The Stress Analysis of Crack Handbook, 3rd ed., New York: ASME Press, 2000.

[19] J. Dundurs, "Edge-bonded dissimilar orhoganal elastic wedges," *J. Appl. Mech.,* vol. 36, pp. 650-652, 1969.

[20] ABAQUS, Analysis User's Manual Version 6.7, Providence: Simulia, 2007.

[21] W. K. Wilson and J. Cherepko, “Analysis of cracks with multiple branches,” *International Journal of Fracture,* vol. 22, pp. 303-315, 1983.

[22] K. T. Faber and A. G. Evans, "Crack deflection processes—II. Experiment," *Acta Metallurgica,* vol. 31, no. 4, pp. 577-584, 1983.

APPENDIX A - UEL

```
CCCCCCCCCCCCCCCCCCCCCCCCCCCCCCCCCCCCCCCCCCCCCCCCCCCCCC
CCCCCCCCCCCCCCC
c from mix_mod-4.f
c                    2D_EPZ.FOR                    c
c     THIS SUBROUTINE IS FOR TRACTION-SEPERATION LAW FOR
MIXED_MODE c
c     IN THIS SUBROUTINE, MODE_I + MODE_II WAS APPLIED AND THE     c
c     FRACTURE CRITERION IS GAMMA = (GI/GIc)+ (GII/GIIc) > 1.0     c
c     STATE VARIABLES ARE USED TO PREVENT FRACTURED ELEMENTS     c
c     FROM BEING USED AGAIN                    c
CCCCCCCCCCCCCCCCCCCCCCCCCCCCCCCCCCCCCCCCCCCCCCCCCCCCCC
CCCCCCCCCCCCCCC
c
  SUBROUTINE UEL(RHS,AMATRX,SVARS,ENERGY,NDOFEL,NRHS,NSVARS,
  1  PROPS,NPROPS,COORDS,MCRD,NNODE,U,DU,V,A,JTYPE,TIME,DTIME,
  2  KSTEP,KINC,JELEM,PARAMS,NDLOAD,JDLTYP,ADLMAG,PREDEF,NPREDF,
  3  LFLAGS,MLVARX,DDLMAG,MDLOAD,PNEWDT,JPROPS,NJPROP,PERIOD)
c
  INCLUDE 'ABA_PARAM.INC'
c
  DIMENSION RHS(MLVARX,*),AMATRX(NDOFEL,NDOFEL),PROPS(*),
  1  SVARS(*),ENERGY(8),COORDS(MCRD,NNODE),U(NDOFEL),
  2  DU(MLVARX,*),V(NDOFEL),A(NDOFEL),TIME(2),PARAMS(*),
  3  JDLTYP(MDLOAD,*),ADLMAG(MDLOAD),DDLMAG(MDLOAD,*),
  4  PREDEF(2,NPREDF,NNODE),LFLAGS(*),JPROPS(*)
c
  DIMENSION C_COOR(2,4), R_COOR(2,4), R_F(8), R_MATRX(8,8)
c
c*********************************************************************
c
   IF(JTYPE.EQ.1)THEN
    scap=PROPS(1)
    rtn1=PROPS(2)
    rtn2=PROPS(3)
    dltn=PROPS(4)
c
    g_ic=0.5D0*scap*(1.0D0-rtn1+rtn2)*dltn
c
    u1=U(3)-U(1)
    u3=U(5)-U(7)
c
    rn_13=u1/dltn
      rn_57=u3/dltn
c
    aht=ABS(COORDS(2,4)-COORDS(2,1))
```

```
      alen=ABS(COORDS(1,1)-COORDS(1,2))
c
      DO 10 i=1,NDOFEL
       DO 11 j=1,NDOFEL
        AMATRX(j,i)=0.0D0
11      CONTINUE
10     CONTINUE
c
c  NODE PAIR 1 AND 3
          IF(rn_13.GT.1.0D0)SVARS(11)=10.0D0
      IF(SVARS(11).GT.1.0D0)THEN
           TN1=0.0D0
           g_crt_13=1.0D0
         ELSE
           CALL ENRG_N(rn_13,scap,rtn1,rtn2,dltn,g_ic,g_i_13)
       g_crt_13=g_i_13/g_ic
           IF(g_crt_13.GT.1.0D0)THEN
            TN1=0.0D0
         SVARS(11)=10.0D0
           ELSE
            CALL TEN(rn_13,scap,rtn1,rtn2,dltn,strn_13,stfn_13)
            TN1=strn_13
         AMATRX(1,1)= aht*stfn_13/3.0D0/dltn
         AMATRX(1,3)=-aht*stfn_13/3.0D0/dltn
         AMATRX(3,1)=-aht*stfn_13/3.0D0/dltn
         AMATRX(3,3)= aht*stfn_13/3.0D0/dltn
         AMATRX(5,1)=-aht*stfn_13/6.0D0/dltn
         AMATRX(5,3)= aht*stfn_13/6.0D0/dltn
         AMATRX(7,1)= aht*stfn_13/6.0D0/dltn
         AMATRX(7,3)=-aht*stfn_13/6.0D0/dltn
       ENDIF
      ENDIF
c
c  NODE PAIR 5 AND 7
          IF(rn_57.GT.1.0D0)SVARS(12)=10.0D0
      IF(SVARS(12).GT.1.0D0)THEN
           TN2=0.0D0
           g_crt_57=1.0D0
         ELSE
           CALL ENRG_N(rn_57,scap,rtn1,rtn2,dltn,g_iC,g_i_57)
       g_crt_57=g_i_57/g_ic
       IF(g_crt_57.GT.1.0D0)THEN
            TN2=0.0D0
         SVARS(12)=10.0D0
           ELSE
            CALL TEN(rn_57,scap,rtn1,rtn2,dltn,strn_57,stfn_57)
            TN2=STRN_57
         AMATRX(1,5)=-aht*stfn_57/6.0D0/dltn
```

```
          AMATRX(1,7)= aht*stfn_57/6.0D0/dltn
          AMATRX(3,5)= aht*stfn_57/6.0D0/dltn
          AMATRX(3,7)=-aht*stfn_57/6.0D0/dltn
          AMATRX(5,5)= aht*stfn_57/3.0D0/dltn
          AMATRX(5,7)=-aht*stfn_57/3.0D0/dltn
          AMATRX(7,5)=-aht*stfn_57/3.0D0/dltn
          AMATRX(7,7)= aht*stfn_57/3.0D0/dltn
        ENDIF
      ENDIF
c
c  FORCE VECTOR
      DO 20 i=1,8
        RHS(i,1)=0.0D0
20     CONTINUE
c
      RHS(1,1)= aht*(2.0D0*TN1+TN2)/6.0D0
      RHS(3,1)=-RHS(1,1)
      RHS(5,1)=-aht*(TN1+2.0D0*TN2)/6.0D0
      RHS(7,1)=-RHS(5,1)
c

      SVARS(1)=u1
      SVARS(2)=u3
      SVARS(3)=TN1
      SVARS(4)=TN2
      SVARS(5)=g_crt_13
      SVARS(6)=g_crt_57
c
    ENDIF
c
c**********************************************************************
c
    IF(JTYPE.EQ.2)THEN
         SCAP=PROPS(1)
         RTN1=PROPS(2)
         RTN2=PROPS(3)
         DLTN=PROPS(4)
         TCAP=PROPS(5)
         RTT1=PROPS(6)
         RTT2=PROPS(7)
         DLTT=PROPS(8)
c
c  INITIALIZE VARIABLES
         G_I_14=0.00D0
         G_II_14=0.00D0
         G_I_23=0.00D0
         G_II_23=0.00D0
         G_CRT_14=0.00D0
```

```
          G_CRT_23=0.00D0
          G_IC=0.5D0*SCAP*(1.0D0-RTN1+RTN2)*DLTN
          G_IIC=0.5D0*TCAP*(1.0D0-RTT1+RTT2)*DLTT
c
          DO 140 I=1,8
            DO 150 J=1,8
              R_MATRX(I,J)=0.0D0
150       CONTINUE
140       CONTINUE
c
c  Prevent "broken" elements from being engaged again
c    SYMBOL_1>1.0 ==> nodes 1&4 have been "separated"
c    SYMBOL_2>1.0 ==> nodes 1&4 have been "separated"
c
          SYMBOL_1=SVARS(11)
          SYMBOL_2=SVARS(12)
c
          DO 100 K1=1,NDOFEL
            DO 110 KRHS=1,NRHS
              RHS(K1,KRHS)=0.0D0
110         CONTINUE
            DO 120 K2=1,NDOFEL
              R_MATRX(K2,K1)=0.0D0
120         CONTINUE
100       CONTINUE
c
          DO 130 I=1,8
            R_F(I)=0.0
            DO 130 J=1,8
              R_MATRX(I,J)=0.0D0
130       CONTINUE
c
c  COMPUTE THE LENGTH AND THICKNESS OF AN EPZ ELEMENT
          ALEN1=SQRT((COORDS(1,1)-COORDS(1,2))**2
     1      +(COORDS(2,1)-COORDS(2,2))**2.0)
          ALEN2=SQRT((COORDS(1,4)-COORDS(1,3))**2
     1      +(COORDS(2,4)-COORDS(2,3))**2.0)
          ALEN=(ALEN1+ALEN2)/2.0D0
          THIK1_0=SQRT((COORDS(1,1)-COORDS(1,4))**2
     1        +(COORDS(2,1)-COORDS(2,4))**2.0)
          THIK2_0=SQRT((COORDS(1,2)-COORDS(1,3))**2
     1        +(COORDS(2,2)-COORDS(2,3))**2.0)
c
        xb=ABS(COORDS(1,1)-COORDS(1,2))/2.0D0
        xh=ABS(COORDS(2,4)-COORDS(2,1))/2.0D0
c
        C_COOR(1,1)=-xb+U(1)
        C_COOR(2,1)=-xh+U(2)
```

```
      C_COOR(1,2)= xb+U(3)
      C_COOR(2,2)=-xh+U(4)
      C_COOR(1,3)= xb+U(5)
      C_COOR(2,3)= xh+U(6)
      C_COOR(1,4)=-xb+U(7)
      C_COOR(2,4)= xh+U(8)
c
c  COMPUTE THE ROTATION ANGLE
        P1_X=(C_COOR(1,1)+C_COOR(1,4))/2.0D0
        P1_Y=(C_COOR(2,1)+C_COOR(2,4))/2.0D0
        P2_X=(C_COOR(1,2)+C_COOR(1,3))/2.0D0
        P2_Y=(C_COOR(2,2)+C_COOR(2,3))/2.0D0
        IF(ABS(P2_X-P1_X).LE.1.0E-10) THEN
          FI=3.14159265/2.0D0
        ELSE
          FI=ATAN((P2_Y - P1_Y)/(P2_X - P1_X))
        ENDIF
c
c  COMPUTE THE COORDINATES IN LOCAL COORDINATE SYSTEM
        R_COOR(1,1)=C_COOR(1,1)*COS(FI)+C_COOR(2,1)*SIN(FI)
        R_COOR(2,1)=-1.0D0*C_COOR(1,1)*SIN(FI)+C_COOR(2,1)*COS(FI)
        R_COOR(1,2)=C_COOR(1,2)*COS(FI)+C_COOR(2,2)*SIN(FI)
        R_COOR(2,2)=-1.0D0*C_COOR(1,2)*SIN(FI)+C_COOR(2,2)*COS(FI)
        R_COOR(1,3)=C_COOR(1,3)*COS(FI)+C_COOR(2,3)*SIN(FI)
        R_COOR(2,3)=-1.0D0*C_COOR(1,3)*SIN(FI)+C_COOR(2,3)*COS(FI)
        R_COOR(1,4)=C_COOR(1,4)*COS(FI)+C_COOR(2,4)*SIN(FI)
        R_COOR(2,4)=-1.0D0*C_COOR(1,4)*SIN(FI)+C_COOR(2,4)*COS(FI)
c
c  COMPUTE THE RELATIVE DISPLACEMENTS IN LOCAL COORDINATE SYSTEM
        DUX1=R_COOR(1,4)-R_COOR(1,1)                    !U(7)-U(1)
        DUX2=R_COOR(1,3)-R_COOR(1,2)                    !U(5)-U(3)
        DUY1=R_COOR(2,4)-R_COOR(2,1)-THIK1_0      !U(8)-U(2)
        DUY2=R_COOR(2,3)-R_COOR(2,2)-THIK2_0      !U(6)-U(4)
        RN_14=DUY1/DLTN
        RT_14=DUX1/DLTT
        RN_23=DUY2/DLTN
        RT_23=DUX2/DLTT
c
c  COMPUTE THE CURRENT THICKNESS OF THE EPZ ELEMENT
        XXL1=R_COOR(1,1)          !COORDS(1,1)+U(1)
        YYL1=R_COOR(2,1)          !COORDS(2,1)+U(2)
        XXL2=R_COOR(1,4)          !COORDS(1,4)+U(7)
        YYL2=R_COOR(2,4)          !COORDS(2,4)+U(8)
        XXR1=R_COOR(1,2)          !COORDS(1,2)+U(3)
        YYR1=R_COOR(2,2)          !COORDS(2,2)+U(4)
        XXR2=R_COOR(1,3)          !COORDS(1,3)+U(5)
        YYR2=R_COOR(2,3)          !COORDS(2,3)+U(6)
        THIK1_1=SQRT((XXL1-XXL2)**2.0+(YYL1-YYL2)**2.0)
```

```
        THIK2_1=SQRT((XXR1-XXR2)**2.0+(YYR1-YYR2)**2.0)
c
c  COMPUTE THE LOCAL STIFFNESS MATRIX AND RESIDUAL FORCES FOR
c  NODE PAIR 1 AND 4
c  CHECK IF CRITICAL DISPLACEMENT IS REACHED: IF EITHER DLTN
c   OR DLTT IS REACHED, THE TOTAL STIFFNESS MATRIX AND RESIDUAL
c   FORCE WILL BE SET TO BE ZERO
c
         IF((RN_14.GT.1.0D0).OR.(ABS(RT_14).GT.1.0D0))SYMBOL_1=10.0D0
         IF(SYMBOL_1.GT.1.0D0)THEN
           TN1=0.0D0
           TT1=0.0D0
      ELSE
           CALL ENRG_T(RT_14, TCAP, RTT1, RTT2, DLTT, G_IIC, G_II_14)
           CALL ENRG_N(RN_14, SCAP, RTN1, RTN2, DLTN, G_IC, G_I_14)
           G_CRT_14=G_I_14/G_IC + G_II_14/G_IIC
           IF (G_CRT_14.GT.1.0D0) THEN
            TN1=0.0D0
            TT1=0.0D0
            SYMBOL_1=10.0D0
       ELSE
           CALL TEN(RN_14,SCAP,RTN1,RTN2,DLTN,STRN_14,STFN_14)
           CALL SHR(RT_14,TCAP,RTT1,RTT2,DLTT,STRT_14,STFT_14)
c
           TN1=STRN_14
           TT1=STRT_14
c
           R_MATRX(1,1)= ALEN*STFT_14/3.0D0/DLTT
         R_MATRX(1,2)= 0.0D0
           R_MATRX(1,7)= -1.0D0*ALEN*STFT_14/3.0D0/DLTT
         R_MATRX(1,8)= 0.0D0

         R_MATRX(2,1)= 0.0D0
         R_MATRX(2,2)= ALEN*STFN_14/3.0D0/DLTN
           R_MATRX(2,7)= 0.0D0
         R_MATRX(2,8)= -1.0D0*ALEN*STFN_14/3.0D0/DLTN

         R_MATRX(3,1)= ALEN*STFT_14/6.0D0/DLTT
         R_MATRX(3,2)= 0.0D0
           R_MATRX(3,7)= -1.0D0*ALEN*STFT_14/6.0D0/DLTT
         R_MATRX(3,8)= 0.0D0

         R_MATRX(4,1)= 0.0D0
         R_MATRX(4,2)= ALEN*STFN_14/6.0D0/DLTN
           R_MATRX(4,7)= 0.0D0
         R_MATRX(4,8)= -1.0D0*ALEN*STFN_14/6.0D0/DLTN
c
       ENDIF
```

```
      ENDIF
c
c  COMPUTE THE LOCAL STIFFNESS MATRIX AND RESIDUAL FORCES FOR
c   NODE PAIR 2 AND 3
c   CHECK IF CRITICAL DISPLACEMENT IS REACHED: IF EITHER DLTN
c   OR DLTT IS REACHED, THE TOTAL STIFFNESS MATRIX AND RESIDUAL
c   FORCE WILL BE SET TO BE ZERO
c
          IF((RN_23.GT.1.0D0).OR.(ABS(RT_23).GT.1.0D0))SYMBOL_2=10.0D0
          IF(SYMBOL_2.GT.1.0D0) THEN
            TN2=0.0D0
            TT2=0.0D0
      ELSE
            CALL ENRG_T(RT_23, TCAP, RTT1, RTT2, DLTT, G_IIC, G_II_23)
            CALL ENRG_N(RN_23, SCAP, RTN1, RTN2, DLTN, G_IC, G_I_23)
            G_CRT_23=G_I_23/G_IC + G_II_23/G_IIC
            IF (G_CRT_23.GT.1.0D0) THEN
              TN2=0.0D0
              TT2=0.0D0
              SYMBOL_2=10.0D0
            ELSE
              CALL TEN(RN_23,SCAP,RTN1,RTN2,DLTN,STRN_23,STFN_23)
              CALL SHR(RT_23,TCAP,RTT1,RTT2,DLTT,STRT_23,STFT_23)
c
              TN2=STRN_23
              TT2=STRT_23
c
              R_MATRX(1,3)= ALEN*STFT_23/6.0D0/DLTT
          R_MATRX(1,4)= 0.0D0
              R_MATRX(1,5)= -1.0D0*ALEN*STFT_23/6.0D0/DLTT
          R_MATRX(1,6)= 0.0D0
c
              R_MATRX(2,3)= 0.0D0
          R_MATRX(2,4)= ALEN*STFN_23/6.0D0/DLTN
              R_MATRX(2,5)= 0.0D0
          R_MATRX(2,6)= -1.0D0*ALEN*STFN_23/6.0D0/DLTN
c
              R_MATRX(3,3)= ALEN*STFT_23/3.0D0/DLTT
          R_MATRX(3,4)= 0.0D0
              R_MATRX(3,5)= -1.0D0*ALEN*STFT_23/3.0D0/DLTT
          R_MATRX(3,6)= 0.0D0

          R_MATRX(4,3)= 0.0D0
          R_MATRX(4,4)= ALEN*STFN_23/3.0D0/DLTN
              R_MATRX(4,5)= 0.0D0
          R_MATRX(4,6)= -1.0D0*ALEN*STFN_23/3.0D0/DLTN
c
            ENDIF
```

```
      ENDIF
c
199   CONTINUE
c
      DO 200 I=1,8
        R_MATRX(5,I)=-1.0D0*R_MATRX(3,I)
        R_MATRX(6,I)=-1.0D0*R_MATRX(4,I)
        R_MATRX(7,I)=-1.0D0*R_MATRX(1,I)
        R_MATRX(8,I)=-1.0D0*R_MATRX(2,I)
200   CONTINUE
c
c COMPUTE THE RESIDUAL FORCES IN LOCAL COORD. SYS.
c
      R_F(1)=(TT1*ALEN/3.0D0+TT2*ALEN/6.0D0)
      R_F(2)=(TN1*ALEN/3.0D0+TN2*ALEN/6.0D0)
      R_F(3)=(TT1*ALEN/6.0D0+TT2*ALEN/3.0D0)
      R_F(4)=(TN1*ALEN/6.0D0+TN2*ALEN/3.0D0)
      R_F(5)=-R_F(3)
      R_F(6)=-R_F(4)
      R_F(7)=-R_F(1)
      R_F(8)=-R_F(2)
c
c FORM THE GLOBAL STIFFNESS MATRIX AND RESIDUAL FORCE
      DO 300 I=1,7,2
        DO 300 J=1,7,2
          AMATRX( I, J) = R_MATRX( I, J)*COS(FI)**2.0D0+
     1                    R_MATRX(I+1,J+1)*SIN(FI)**2.0D0-
     2                    R_MATRX( I,J+1)*SIN(FI)*COS(FI)-
     3                    R_MATRX(I+1, J)*SIN(FI)*COS(FI)
c
          AMATRX(I+1, J) = R_MATRX( I, J)*SIN(FI)*COS(FI)-
     1                     R_MATRX(I+1,J+1)*SIN(FI)*COS(FI)-
     2                     R_MATRX( I,J+1)*SIN(FI)**2.0D0+
     3                     R_MATRX(I+1, J)*COS(FI)**2.0D0
c
          AMATRX( I,J+1) = R_MATRX( I, J)*SIN(FI)*COS(FI)-
     1                     R_MATRX(I+1,J+1)*SIN(FI)*COS(FI)+
     2                     R_MATRX( I,J+1)*COS(FI)**2.0D0-
     3                     R_MATRX(I+1, J)*SIN(FI)**2.0D0

c
          AMATRX(I+1,J+1) = R_MATRX( I, J)*SIN(FI)**2.0D0+
     1                     R_MATRX(I+1,J+1)*COS(FI)**2.0D0+
     2                     R_MATRX( I,J+1)*SIN(FI)*COS(FI)+
     3                     R_MATRX(I+1, J)*SIN(FI)*COS(FI)
c
300   CONTINUE
c
```

```
          DO 310 I=1,7,2
            RHS( I ,1)=R_F(I)*COS(FI) - R_F(I+1)*SIN(FI)
            RHS(I+1,1)=R_F(I)*SIN(FI) + R_F(I+1)*COS(FI)
310       CONTINUE
c
c UPDATE INTERNAL VARIABLES
          SVARS(11)=SYMBOL_1
          SVARS(12)=SYMBOL_2
c
      SVARS(2)=TN1
      SVARS(4)=TT1
          SVARS(6)=TN2
          SVARS(8)=TT2
c
      SVARS(9)=FI
c
          SVARS(18)=G_I_14
          SVARS(19)=G_II_14
          SVARS(20)=G_I_23
          SVARS(21)=G_II_23
c
          SVARS(22)=G_CRT_14
          SVARS(23)=G_CRT_23
c
     ENDIF
c
     RETURN
     END
c
c
c SUBROUTINES
c
     SUBROUTINE SHR(RTT,TAO,RTT1,RTT2,DLTT,STRT,STFT)
       IMPLICIT DOUBLE PRECISION(A-H, O-Z)
       IF(ABS(RTT).LE.RTT1)THEN
         STRT=TAO*RTT/RTT1
         STFT=TAO/RTT1
       ELSEIF((ABS(RTT).GT.RTT1).AND.(ABS(RTT).LE.RTT2))THEN
         STRT=TAO*(ABS(RTT)/RTT)
         STFT=0.0D0
       ELSEIF((ABS(RTT).GT.RTT2).AND.(ABS(RTT).LE.1.0D0))THEN
         STRT=TAO*(1.0D0-ABS(RTT))/(1.0D0-RTT2)*(ABS(RTT)/RTT)
            STFT=-TAO/(1.0D0-RTT2)
       ELSEIF(ABS(RTT).GT.1.0D0)THEN
         STRT=0.0D0
         STFT=0.0D0
       ENDIF
     RETURN
```

```
      END
c
      SUBROUTINE TEN(RTN,SCAP,RTN1,RTN2,DLTN,STRN,STFN)
       IMPLICIT DOUBLE PRECISION(A-H, O-Z)
       IF(RTN.LE.RTN1)THEN
        STRN=SCAP*RTN/RTN1
        STFN=SCAP/RTN1
       ELSEIF((RTN.GT.RTN1).AND.(RTN.LE.RTN2))THEN
        STRN=SCAP
        STFN=0.0D0
       ELSEIF((RTN.GT.RTN2).AND.(RTN.LE.1.0D0))THEN
        STRN=SCAP*(1.0D0-RTN)/(1.0D0-RTN2)
        STFN=-1.0D0*SCAP/(1.0D0-RTN2)
       ELSEIF(RTN.GT.1.0D0)THEN
        STRN=0.0D0
        STFN=0.0D0
       ENDIF
      RETURN
      END
c
      SUBROUTINE ENRG_N(RTN, SCAP, RTN1, RTN2, DLTN, G_IC, G_I)
       IMPLICIT DOUBLE PRECISION(A-H, O-Z)
       IF(RTN.LE.1.0E-10)THEN
        G_I=0.0D0
       ELSEIF((RTN.GT.1.0E-10).AND.(RTN.LE.RTN1))THEN
        G_I=0.5D0*SCAP*RTN*RTN*DLTN/RTN1
       ELSEIF((RTN.GT.RTN1).AND.(RTN.LE.RTN2))THEN
        G_I=0.5D0*SCAP*RTN1*DLTN + SCAP*(RTN-RTN1)*DLTN
       ELSEIF((RTN.GT.RTN2).AND.(RTN.LE.1.0D0)) THEN
        G_I=DLTN*((RTN-2.0D0)*RTN+RTN1-RTN1*RTN2+(RTN2)**2)*SCAP/
     1      (2.0D0*(RTN2-1.0D0))
       ELSEIF(RTN.GT.1.0D0) THEN
        G_I=G_IC
       ENDIF
      RETURN
      END
c
      SUBROUTINE ENRG_T(RTT, TAO, RTT1, RTT2, DLTT, G_IIC, G_II)
       IMPLICIT DOUBLE PRECISION(A-H, O-Z)
       IF(ABS(RTT).LE.1.0E-10) THEN
        G_II=0.0D0
       ELSEIF((ABS(RTT).GT.1.0E-10).AND.(ABS(RTT).LE.RTT1)) THEN
        G_II=0.5D0*TAO*ABS(RTT)*ABS(RTT)*DLTT/RTT1
       ELSEIF((ABS(RTT).GT.RTT1).AND.(ABS(RTT).LE.RTT2)) THEN
        G_II=0.5D0*TAO*RTT1*DLTT + TAO*(ABS(RTT)-RTT1)*DLTT
       ELSEIF((ABS(RTT).GT.RTT2).AND.(ABS(RTT).LE.1.0D0)) THEN
        G_II=DLTT*((ABS(RTT)-2.0D0)*ABS(RTT)+RTT1-RTT1*RTT2+(RTT2)**2)
     1      *TAO/(2.0D0*(RTT2-1.0D0))
```

```
  ELSEIF(ABS(RTT).GT.1.0D0) THEN
    G_II=G_IIC
  ENDIF
RETURN
END
```

APPENDIX B – LEFM Two-Geometry Curves Derivation

Here, the work of He and Hutchinson [6] is adapted to the fracture model studied in present work in order to make comparisons and draw conclusions. At fracture, He and Hutchinson [6] formulate

$$G_p = \frac{1-\nu_s}{2\mu_s} K_I^2 \qquad (10)$$

for the penetrating direction, and

$$G_d = \left(\frac{1-\nu_s}{\mu_s} + \frac{1-\nu_f}{\mu_f}\right)\left(\frac{K_I^2 + K_{II}^2}{4\cosh^2(\pi\varepsilon)}\right) \qquad (11)$$

for the deflecting direction where K is the stress intensity factor (with I and II representing mode-I and mode-II respectively), ν is Poisson's ratio, μ is shear modulus, ε is an oscillation index dependent on the Dundurs parameter, β, from Dundurs [19]. Also, subscripts s, p, i, f represent substrate, penetrating, interface, and film respectively.

The results of He and Hutchinson [6] can be expanded to show the fracture load associated with this two-geometry approach. First, from LEFM, the Mode-I critical energy release rate (G_{Ic}) is defined to be:

$$G_{Ic} = \Gamma_I = \frac{K_I^2}{\bar{E}} \tag{12}$$

where Γ_I is the mode-I material toughness and $\bar{E}$ is the elastic modulus. Next, a solution for a semi-infinite edge-crack loaded axially (here, the solution for crack length ten times smaller than ligament length is used) from Tada et al. [18] is defined to be:

$$K_I = 1.197\sigma_{applied}\sqrt{\pi h} \tag{13}$$

where $\sigma_{applied}$ is the remote applied tensile stress and h is the crack length. Combining equations (12) and (13) the following relationship can be formed:

$$\sqrt{\frac{1}{\Gamma_I}} = \frac{\sqrt{\bar{E}}}{K_I} = \frac{1}{1.197\sigma_{applied}}\sqrt{\frac{\bar{E}}{\pi h}} \tag{14}$$

Next, a dimensionless group which normalizes a remote applied tensile stress by a crack length, elastic modulus, and toughness can be defined as:

$$\sigma_{applied}\sqrt{\frac{h}{\bar{E}\Gamma_i}} \equiv \text{Fracture Load} \qquad (15)$$

Next, by combining equations (14) and (15) the fracture load is becomes

$$\left(\sigma_{applied}\sqrt{\frac{h}{\bar{E}\Gamma_i}}\right)_p = \sigma_{applied}\sqrt{\frac{h}{\bar{E}}}\sqrt{\frac{\Gamma_s}{\Gamma_s}}\sqrt{\frac{1}{\Gamma_i}} = \frac{1}{1.197\sqrt{\pi}}\sqrt{\frac{\Gamma_s}{\Gamma_i}} \qquad (16)$$

in the penetrating direction, and

$$\left(\sigma_{applied}\sqrt{\frac{h}{\bar{E}\Gamma_i}}\right)_d = 0.923 \qquad (17)$$

in the deflecting direction for Dundurs parameters both equal to zero.

APPENDIX C – LEFM Transition Curve Derivation

Here, an analytical LEFM derivation of transition is derived. We start with results from Wilson and Cherepko [21] for stress intensity factors associated with branched kinks at the end of a main crack. The kinks are positioned at ninety degree angles with respect to each other like that pictured in Figure 7. In this work, percentage stress intensity factors for mode-I and mode-II, k_{I} and k_{II}, are developed for the penetrating and deflecting kinks; these values are percentage intensities of the main crack stress intensity factor, K_{I}. Wilson and Cherepko [21] formulate:

$$k_{\mathrm{I}}/_{K_{\mathrm{I}}} = 0.925\Big|_{\mathrm{Penetration}} \tag{18}$$

$$k_{\mathrm{II}}/_{K_{\mathrm{I}}} = 0\Big|_{\mathrm{Penetration}} \tag{19}$$

$$k_{\mathrm{I}}/_{K_{\mathrm{I}}} = 0.270\Big|_{\mathrm{Deflection}} \tag{20}$$

$$k_{\mathrm{II}}/_{K_{\mathrm{I}}} = 0.125\Big|_{\mathrm{Deflection}} \tag{21}$$

To arrive at a single percentage stress intensity for each kink, the magnitude between mode-I and mode-II is taken:

$$\sqrt{{k_{\mathrm{I}}}^2 + {k_{\mathrm{II}}}^2}\Big|_{\text{Penetration}} = 0.925\, K_{\mathrm{I}} \qquad (22)$$

$$\sqrt{{k_{\mathrm{I}}}^2 + {k_{\mathrm{II}}}^2}\Big|_{\text{Deflection}} = 0.298\, K_{\mathrm{I}} \qquad (23)$$

Next, taking into account that Wilson and Cherepko [21] used a plane strain formulation in which $\bar{E} = \frac{E}{1-\nu^2}$, we sum the total energy release rate for all three kinks using equation (12) for $\nu = 0.3$:

$$\begin{aligned} G &= G_{\text{Penetration}} + 2G_{\text{Deflection}} \\ &= \frac{(0.925\, K_{\mathrm{I}})^2}{E}(1-\nu^2) + 2 * \frac{(0.298\, K_{\mathrm{I}})^2}{E}(1-\nu^2) = \frac{0.9402{K_{\mathrm{I}}}^2}{E} \end{aligned} \qquad (24)$$

This can be rewritten as:

$$K_{\mathrm{I}}^2 = 1.064EG \qquad (25)$$

Equation (13) can be rewritten as:

$$K_I^2 = 1.4328\sigma^2\pi h \quad (26)$$

Equations (25) and (26) can be combined such that,

$$1.064EG = 1.4328\sigma^2\pi h \quad (27)$$

Next, we assume the system is taken until the energy release rate, G, is taken until fracture ($G = \Gamma_{\text{Substrate}} + 2\Gamma_{\text{Interface}}$). Equation (27) can then be rewritten:

$$G = \Gamma_{\text{Substrate}} + 2\Gamma_{\text{Interface}} = 1.347\frac{\sigma^2\pi h}{E} \quad (28)$$

Finally, we solve for normalized fracture load:

$$\sigma_{applied}\sqrt{\frac{h}{E\Gamma_{\text{Interface}}}} = 0.486\sqrt{\frac{\Gamma_{\text{Substrate}}}{\Gamma_{\text{Interface}}} + 2} \quad (29)$$